New Mexico Geological Society

Downloaded from: https://nmgs.nmt.edu/publications/guidebooks/51

Chronology and geochemistry of the Boot Heel volcanic field, New Mexico

William C. McIntosh and Charles Bryan
2000, pp. 157-174. https://doi.org/10.56577/FFC-51.157

in:

Southwest Passage: A trip through the Phanerozoic, Lawton, T. F.; McMillan, N. J.; McLemore, V. T.; [eds.], New Mexico Geological Society 51 st Annual Fall Field Conference Guidebook, 282 p. https://doi.org/10.56577/FFC-51

This is one of many related papers that were included in the 2000 NMGS Fall Field Conference Guidebook.

Annual NMGS Fall Field Conference Guidebooks

Every fall since 1950, the New Mexico Geological Society (NMGS) has held an annual Fall Field Conference that explores some region of New Mexico (or surrounding states). Always well attended, these conferences provide a guidebook to participants. Besides detailed road logs, the guidebooks contain many well written, edited, and peer-reviewed geoscience papers. These books have set the national standard for geologic guidebooks and are an essential geologic reference for anyone working in or around New Mexico.

Free Downloads

NMGS has decided to make peer-reviewed papers from our Fall Field Conference guidebooks available for free download. This is in keeping with our mission of promoting interest, research, and cooperation regarding geology in New Mexico. However, guidebook sales represent a significant proportion of our operating budget. Therefore, only *research papers* are available for download. *Road logs*, *mini-papers*, and other selected content are available only in print for recent guidebooks.

Copyright Information

Publications of the New Mexico Geological Society, printed and electronic, are protected by the copyright laws of the United States. No material from the NMGS website, or printed and electronic publications, may be reprinted or redistributed without NMGS permission. Contact us for permission to reprint portions of any of our publications.

One printed copy of any materials from the NMGS website or our print and electronic publications may be made for individual use without our permission. Teachers and students may make unlimited copies for educational use. Any other use of these materials requires explicit permission.

This page is intentionally left blank to maintain order of facing pages.

CHRONOLOGY AND GEOCHEMISTRY OF THE BOOT HEEL VOLCANIC FIELD, NEW MEXICO

WILLIAM C. McINTOSH[1] and CHARLES BRYAN[2]

[1]New Mexico Bureau of Mines and Mineral Resources, New Mexico Institute of Mining and Technology, Tech, 801 Leroy Pl., Socorro, NM, 87801, mcintosh@nmt.edu ;
[2]MS 1395, Sandia National Laboratory, 4100 National Parks Highway, Carlsbad, NM, 88220, crbryan@sandia.gov

ABSTRACT—High-precision $^{40}Ar/^{39}Ar$ geochronology, paleomagnetic analyses, and geochemical studies allow reliable correlations of regional ignimbrites (ash-flow tuffs) that define a time-stratigraphic framework for the late Eocene–Oligocene Boot Heel volcanic field of southwestern New Mexico. Previous studies identified and locally correlated many of the field's large-volume ignimbrites, but were unable to establish sufficient regional correlations to develop an integrated stratigraphy. New $^{40}Ar/^{39}Ar$ dating results from single-crystal and multigrain (bulk) sanidine provide precise (±0.25–0.5%) ages for sanidine-bearing rhyolite to rhyodacite ignimbrites and lavas. Paleomagnetic polarity and direction data, together with geochemical analyses, augment regional correlations based on $^{40}Ar/^{39}Ar$ data. Nine large-volume ignimbrites in the Boot Heel volcanic field erupted in two distinct pulses (35.2–32.7 Ma and 27.6–26.8 Ma) separated by a 5.1-m.y. hiatus in ignimbrite activity. Source calderas are recognized for eight of the ignimbrites, and seven of the ignimbrites include widespread regional outflow facies. Caldera activity shifted from east to west during the life span of the volcanic field. Local volcanic units intercalated with the regional ignimbrites include basaltic, andesitic, dacitic, and rhyolitic lava flows and pyroclastic rocks. Some of these units are associated with regional ignimbrite calderas. The early and late pulses of ignimbrite volcanism are geochemically distinct. The 35.2–32.7-Ma ignimbrites are in general less evolved, contain more hydrous minerals, have lower concentrations of incompatible trace elements, and more shallowly dipping trace element enrichment/depletion patterns than the three 27.6–26.8-Ma ignimbrites. The younger ignimbrites were apparently derived from less-volatile-rich magmas as a consequence of progressive change from subduction to extensional tectonic environments between 32.7 Ma and 27.6 Ma. Because of the lower volatile contents, higher degrees of fractionation occurred prior to cauldron-forming eruptions.

INTRODUCTION

During latest Eocene–early Miocene time, southwestern North America experienced widespread silicic volcanism related to post-Laramide cessation of subduction along the western margin of the North American plate (Lipman et al., 1972). Caldera volcanism during this interval was distributed in a chain of large silicic volcanic fields extending southward from Colorado into Mexico (Fig. 1). The most extensively studied of these volcanic fields are the San Juan field in Colorado (Lipman et al., 1978), the Mogollon-Datil field in New Mexico (McIntosh et al., 1992a), and the Trans-Pecos field in Texas (Henry et al., 1994). Less well known is the subject of this paper: the Boot Heel volcanic field in the southwestern corner of New Mexico and adjacent Arizona (Figs. 1, 2, Table 1). The Boot Heel field is in the Basin-and-Range Province, between the Sierra Madre volcanic province to the south, and the Mogollon-Datil volcanic field to the north (Bryan, 1995). The boundaries of the Boot Heel field and adjacent fields have not been formally established, but are here considered to be near highway I-10 in the north and near the U.S./Mexico border to the south (Fig. 1).

Previous studies in the Boot Heel volcanic field (Table 2) have mapped more than 40 ignimbrite units and dozens of basaltic to rhyolitic lavas, and have proposed at least 13 calderas, but have failed to establish an accurate composite stratigraphic framework. Most well-mapped units have been largely confined to single, isolated mountain ranges, and attempts to correlate units from range to range have been only partially successful (Erb, 1979; Elston, 1983). Although caldera-derived, large-volume regional ignimbrites (ash-flow tuffs) are potentially ideal time-stratigraphic marker units (Hildreth and Mahood, 1985), several factors complicate their correlation, particularly in areas like the Boot Heel field, where discontinuous Basin-and-Range exposures limit correlations based on mapping of continuous outcrops. Different ignimbrites may be lithologically identical, whereas individual ignimbrites may exhibit strong compositional variations due to magma-chamber zonation. Ignimbrite outflow facies are commonly emplaced early in the eruption, whereas exposed intracaldera ignimbrite commonly represents chemically distinct later-erupted magma. Flow segregation of phenocrysts, pumice fragments, and fine ash commonly results in variations in the texture and crystal content of proximal and distal outflow facies. Variations in welding, devitrification, and alteration can cause spatial variations in textures within individual ignimbrites. In addition, individual outflow sheets may locally consist of multiple cooling units, and distal facies of ignimbrites may extend from one volcanic field into neighboring fields. Studies in other volcanic fields have demonstrated that high-precision $^{40}Ar/^{39}Ar$ dating can help solve many ignimbrite correlation problems, especially if combined with other methods (Hildreth and Mahood, 1985; McIntosh et al., 1992a). This paper describes how high-precision $^{40}Ar/^{39}Ar$ dating, together with paleomagnetic data and comprehensive chemical and petrographic analyses, have been used to develop a composite time-stratigraphic framework for the Boot Heel volcanic field and to model its geochemical evolution.

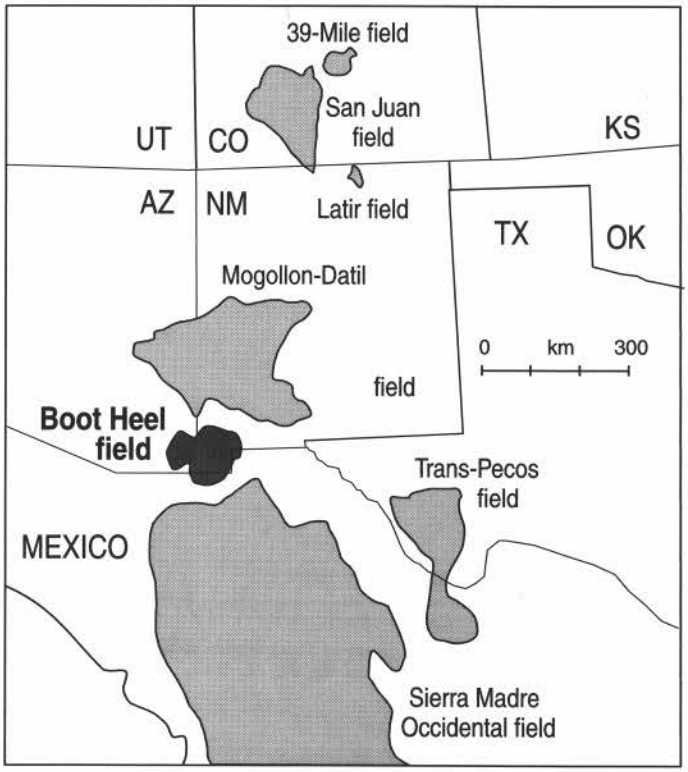

FIGURE 1. Late Eocene/Oligocene silicic volcanic fields in western North America.

TABLE 1. Major ignimbrites and calderas in the Boot Heel volcanic field.

Ignimbrite	n (samples dated)	Mineral	Age (Ma)	±2σ	Rounded age (Ma)	Polarity	Caldera	Volume (km³)	Max. thickness (m)	Silica range (anhydrous)	Evidence for caldera	References
Rhyolite Canyon Tuff	3	S	26.76 ±	0.20	26.8	N	Turkey Creek	650	1500	73–77	123456789	1, 2
Park Tuff	7	S	27.44 ±	0.08	27.4	N	Clanton Draw?	120	75	74–78	8?	3, 4
tuff of Horseshoe Canyon	17	S	27.63 ±	0.03	27.6	N	Portal	140	500	64–77	12456789	5
Gillespie Tuff	17	S	32.72 ±	0.04	32.7	N	Geronimo Trail	640	500	68–76	1249	4
tuff of Black Bill Canyon	1	B	33.57 ±	0.18	33.5*	R	Animas Peak	35	350	62–67	129	4
Oak Creek Tuff	16	S	33.50 ±	0.07	33.5	R	Juniper	520	500	65–75	1(2?)456(7?)89	4
tuff of Steins	11	S	34.45 ±	0.08	34.4	N	Steins	115	350	70–76	1456789	6
Bluff Creek Tuff	4	S	35.08 ±	0.08	35.1	N	Tullous	330	670	72–74	19	4
tuff of Woodhaul Canyon	1	B	35.23 ±	0.13	35.2	R	Muir	50	425	68–69	1(2?)456(8?)	7

notes:
*Age of biotite from Black Bill Canyon rounded down to reflect well constrained age of underlying Oak Creek Tuff.

Evidence for caldera
1 Thickness > 300 m
2 Exposed structural margin
3 Exposed topographic margin
4 Megabreccia/mesobreccia
5 Resurgence
6 Resurgent intrusion
7 Structural boundary intrusions
8 Moat rhyolite and/or dacite volcanism
9 Pervasive alteration of intracaldera ignimbrite

References
1 Marjaniemi (1969)
2 du Bray et al. (1999)
3 McIntyre (1988
4 Erb (1979)
5 Bryan (1988)
6 Richter et al. (1990)
7 Elston et al. (1978)

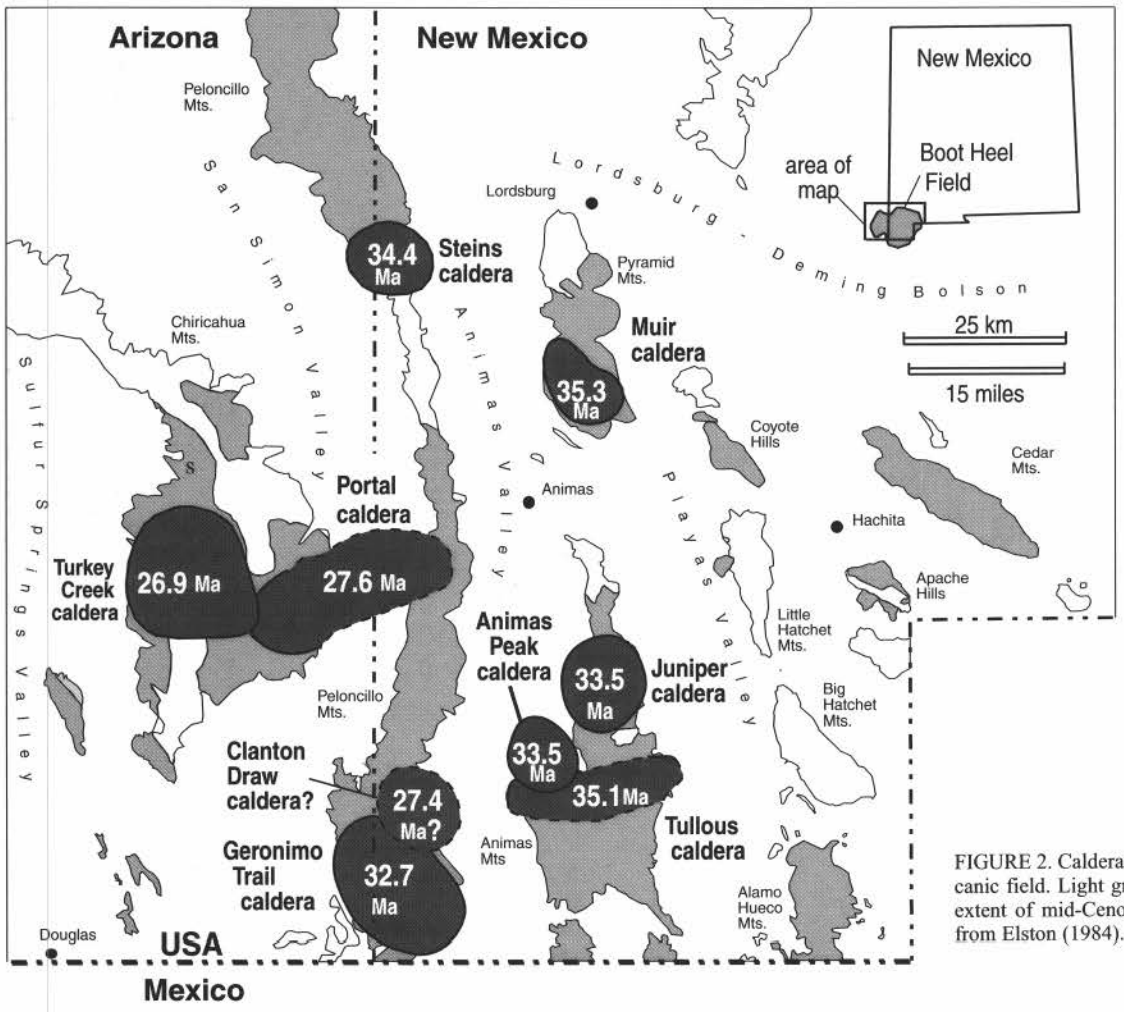

FIGURE 2. Calderas (dark gray) in the Boot Heel volcanic field. Light gray shading indicates approximate extent of mid-Cenozoic volcanic outcrops. Modified from Elston (1984).

Previous work

Previous work in the Boot Heel area (Table 2) has largely been reconnaissance-style mapping. Earliest studies were concerned primarily with the pre-Tertiary rocks, usually with emphasis on their role as hosts for mineral deposits. Mid-Cenozoic volcanic rocks in the Boot Heel area were shown to rest primarily on locally deformed andesitic lavas and intermediate-to-silicic intrusive rocks emplaced during Laramide compression. Beginning in the 1950s, mid-Tertiary volcanic sections in parts of the Peloncillo, Pyramid, and Animas Mountains were described (Table 2). Systematic mapping of the entire field, attempts at regional correlation by K-Ar and fission-track dating, and efforts to define the cauldron sources of the major ignimbrite sheets began in the late 1960s and 1970s. Attempts to define a composite stratigraphy for the entire field (Deal et al., 1978; Erb, 1979; Elston, 1983, 1984) were of limited success, in large part because of the imprecision of conventional K-Ar and fission-track dating. Table 3 summarizes the local stratigraphic sequences identified by previous workers.

$^{40}Ar/^{39}Ar$ methods and results

Mineral separates from a total of 115 samples of tuffs and lavas from the Boot Heel field were dated by $^{40}Ar/^{39}Ar$ methods. One or more samples were collected from most of the ignimbrites and many of the rhyolitic lavas exposed in Boot Heel mountain ranges; these samples represent most of the named rhyolitic units mapped by previous workers (Table 3). Sanidine, well established as the premier volcanic mineral for high-precision dating (Deino and Potts, 1990; McIntosh et al., 1990), was analyzed from 111 of these samples, and biotite or plagioclase was analyzed from four rhyodacitic samples that lacked sanidine. Resistance-furnace step-heating methods were initially used to date 64 of the samples in the U.S. Geological Survey (USGS) $^{40}Ar/^{39}Ar$ facility in Reston, Virginia. All other samples were analyzed at the New Mexico Geochronology Research Laboratory by single-crystal laser-fusion (sanidine and plagioclase) or laser step heating (biotite). Fish Canyon Tuff sanidine with an assumed age of 27.84 Ma (Deino and Potts, 1990) was used as a monitor throughout the study. Details of separation and analytical methods are in McIntosh et al. (1990), McIntosh and Chamberlin (1994), and McIntosh and Bryan (2000). Results are summarized in Figs. 3, 4, Table 1, and Appendix 1. Complete analytical data are in McIntosh and Bryan (2000).

Both single-crystal laser-fusion and resistance-furnace step-heating Ar analyses yielded precise, accurate ages for sanidine bearing units. The precision ($\pm 2\sigma$) for most of the analyses is between $\pm$ 0.25% and $\pm$ 0.5%. Close agreement among multiple samples from the same unit and agreement with stratigraphic order (Figs. 4, 5, Appendix 1) attest to the accuracy of the sanidine data, relative to the assumed monitor ages. $^{40}Ar/^{39}Ar$ dates were also obtained from biotite or plagioclase from four samples, but are less precise and less accurate than the sanidine results, as indicated by large analytical uncertainties and, in some cases, poor agreement with stratigraphy. Following sections discuss $^{40}Ar/^{39}Ar$ results in the context of the stratigraphic framework of ignimbrites in the Boot Heel volcanic field. Analyses are now in progress to re-date previously step-heated sanidines using single-crystal laser-fusion techniques. This work will eliminate the possibility of undetected xenocrystic contamination, which cannot be entirely ruled out in current data from multi-grain (bulk) sanidine separates.

Paleomagnetic methods and results

In addition to $^{40}Ar/^{39}Ar$ geochronology, paleomagnetic analyses were performed on field-drilled oriented cores from 126 sites in the Boot Heel volcanic field. Field sampling techniques and analytical methods were identical to those described in McIntosh (1991). Accurate paleomagnetic remanence directions were obtained for 116 of these sites. The paleomagnetic polarity results are summarized in Table 1 and Figures 4 and 5. Remanence directions are listed in Appendix 1, but are not discussed in this paper.

Geochemistry methods and results

Geochemical analyses were performed on a total of 131 volcanic rock samples from the Boot Heel volcanic field, using methods detailed in Bryan (1995). One or two representative samples were collected from each lava flow, and ignimbrite units were more thoroughly sampled to allow assessment of within-unit compositional variations. Major element abundances, and the trace elements Rb, Sr, Y, Zr, Nb, and Ba, were determined by X-ray fluorescence analysis. Ferrous iron (FeO) was determined independently by wet chemical methods. Water content for each sample was determined by dehydration at 110°C (H_2O^-) and 1000°C (H_2O^+). A subset of samples (73) was analyzed for rare-earth elements (REE) (La, Ce, Nd, Sm, Eu, Tb, Dy, Yb, and Lu) and for Sc, Cs, Hf, Ta, Th, and U, using instrumental neutron activation analysis (INAA). Rb and Sr isotope analyses were performed on 105 samples, and Nd, Sm, and Pb isotope analyses on 14 samples. Geochemical results are summarized in Tables 1 and 4 and other figures, and are discussed below. Complete analytical results and estimates of analytical precision and accuracy are available in McIntosh and Bryan (2000) and Bryan (1995).

TIME STRATIGRAPHIC FRAMEWORK

The time-stratigraphic framework determined for the Boot Heel volcanic field consists of nine regional, ignimbrite sheets, which are inter-

TABLE 2. References to previous work in the Boot Heel volcanic field.

Range or study	Previous work
Chiricahua Mountains	Raydon (1952), Enlows (1951,1955), Sabins (1957), Fernandez and Enlows (1966), Marjaniemi (1969), Drewes and Williams (1973), Drewes (1982), Latta (1983), Pallister and du Bray (1989, 1994), Pallister et al. (1994), du Bray and Pallister (1994a, b), Bryan (1988, 1989).
Peloncillo Mountains	Gillerman (1958), Wrucke and Bromfield (1961), Deal (unpub. map, summarized in Deal et al. [1978]), Armstrong et al. (1978), Erb (1979), Gebben (1979), Drewes and Thorman (1980a and b), Hayes, (1982), Elston (1983), Hudson (1984), Smith (1987), McIntyre (1988), Richter et al. (1990).
Pyramid Mountains	Lasky (1938), Flege (1959), Thorman and Drewes (1978), Elston et al. (1978).
Animas Mountains	Zeller and Alper (1965), Drewes (1986), Erb (1979).
Coyote Hills and Little Hatchet Mountains	Lasky (1947), Zeller (1970), Thorman (1977).
Alamo Hueco Mountains and Dog Mountains	Zeller (1958), Reiter (1980).
Apache Hills	Strongin (1958), Peterson (1976).
Regional studies	Deal et al. (1978), Erb (1979), Elston (1983, 1984).
Radiometric age tabulations	Marvin et al. (1978), Marvin and Dobson (1979).

TABLE 3. Stratigraphic sequences and nomenclature of previous workers, including unit names and abbreviations used in Table 4 and Appendix 1.

Range:	Chiricahua Mountains	Peloncillo NW	Peloncillo N	Pyramid Mountains	Coyote Hills
Ref:	Bryan (1988)	Drewes and Thorman (1980b)	Richter et al. (1990)	Elston et al. (1979)	Thorman (1983)
Units:	Tfv-volcs of Fife Canyon	Tw-Weatherby Canyon Formation	**Thrr-rhy of Horseshoe Ranch**	Trt-*Rimrock Mountain Group*	Tb-basalt.
	Tfru-upper rhy	Twur-upper rhy	Tdp-dac plug	**Trt8-tuff 8 (1)**	Tm-moonstone tuff
	Tfql-quartz latite	**Twg-Granddad Windmill**	Ta-andesite flows	Trb3-basalt 3	*Tru-rhy welded tuff*
	Tftb-tuff breccia	**Twe-1117 Mountain (2)**	**Taf-ash flow tuff**	**Trt7-tuff 7 (11)**	**Tr1,Tr2,Tr3**
	Tfrl-lower rhy	Twm-Martin Draw	Tmr-rhy of Midway Peak	Trb2-basalt 2	Tcs,Tcp-rhy of Coyote Peak
	Tflp-latite porphyry	Twh-Hackett Canyon	Tdd-dac dikes and plug	**Trt6-tuff 6 (4)**	*Tp- volcs of Pothook,*
	Trc-Rhyolite CanyonTuff	**Twlr-lower rhy**	Ttu-andesite and dac flows	**Trt5-tuff 5 (2)**	Tpc-clastic tuffaceous unit
	Tpv-volcs of Pothole Canyon	pT-deformed pre-Tertiary units	**Tmd-dac of McKenzie Peak**	**Trt4-tuff 4 (5)**	Tpqf-quartz latite lava
	Tpva-andesite		*Orange Butte, FBP*	**Trt3-tuff 3**	**Tplt-lithic tuff unit (2)**
	Tpvr-rhy		Tob,Tod,Tor-rhy,dac,andesite	Trb1-basalt 1	**Tpqw-quartz latite tuff**
	Tldp-latite of Darnell Peak		*Horsecamp FBP*	**Trt2-tuff 2**	*Tptu-rhy tuff*
	Thc-tuff of Horseshoe Canyon		Thb, Thd,Thr-rhy,dac,andesite	**Trt1-tuff 1**	**Tpt1,Tpt2,Tptw**
	Tcc-rhy of Cave Creek		*ring-fracture FBP*	Tp-rhy of Pyramid Peak	**Tpp-purple rhy lithic tuff**
	TKa-andesite of Sulfur Draw		Trr,Trd,Trhp-rhy, dac, hbl porph	**Tu-latite of Uhl Well**	**Tprt-rhy tuffs of CoyoteTank**
			Tst-tuff of Steins	Tg-tuff of Graham Well	Tka,TKi-andesite of Bertiglio-Merrill Ranch
			Tid-dac of Indian Springs	**Tw-tuff of Woodhaul Canyon**	
			Tsla, Tsua-lower and upper andesite units	Tj-rhy of Jose Placencia Canyon	
			Tsr,Tsp-rhy of Doubtful Canyon	TKg-andesite of Gore Canyon	
			Tab-b/a	TKs-andesite of Shakespeare	
			Tmp-massive pyroclastic deposits	Th-andesite of Holtcamp Canyon	
			Tba-b/a		
			Tdf,Trb- dac FB	Drewes and Thorman, 1980a	
			Td-dac	Tm-rhyolite of Mudhole Draw	
			TKad-andeite and dac	**Trw-rhyolite ash-flow welded tuff (2)**	
				Tr-rhyolite tuff(2)	
				Trd-rhyolite tuff of Dogshead	
				Tka	

Range:	Peloncillo SW	Peloncillo S	Animas Mountains	Alamo Hueco and Dog Mountains	Apache Hills
Ref:	Deal (1979, unpub. map).	Erb (1979)	Erb (1979)	Reiter (1980)	Peterson (1976)
Units:	**Tda-Double Adobe Latite**	**Tda-Double Adobe Latite**	Tsp-basalt of San Luis Pass.	Tbb-basalt of Beak Creek.	Twr-rhy of Wamels Pond
	Tmt-moonstone tuff	**Tdc-tuff of Dutchman Canyon**	Tda-Double Adobe Canyon	Tp-ParkTuff	Tfr-flow-banded rhy
	Tsc-tuff of Skeleton Canyon	Tav-cong of Animas Valley	**Tpc-rhy of Pine Canyon**	Tbab-b/a of Bull canyon	Trp-rhy porphyry
	Trt-tuff of Trail Creek	Twc-tuff of Whitmire Canyon	**Tpt-rhy of Packers Trail**	**Tg-GillespieTuff**	Tqm-quartz monzonite stock
	Tap-unit of Antelope Pass	**Tcd-rhy of Clanton Draw**	Tsm-bas of San Luis Mountains	**Tgr-tuff of Gray Ranch**	*Chapo Formation*
	Tocl-latite of Owl Can yon	**Tsc-tuff of Skeleton Canyon**	**Tp-ParkTuff (3)**	**Toc-Oak Creek Tuff**	Tcba-basalt and andesite
	Tom-dac of Outlaw Mountain	Tcr-fanglomerate of Cowan Ranch	Twm-bas of Whitewater Mountains	Twc-tuff of Wood canyon	Tcqu-upper quartz latite
	Tsr-rhy of Sloan Ranch	Tsq-quartz latite of Spring of Contention	Tcp-andesite of Center Peak	Tbc-Bluff Creek Formation	Tca-andesite
	Tws-tuff of Woodchopper Canyon	Thr-dac of Ruins Hill	**Tg-GillespieTuff (8?)**	Tec-b/a of Emory Canyon	Tcql-basal quartz latite
	Tbt-biotite-rich tuff	**Twg-rhy of White Gate**	**Tgr-tuff of Gray Ranch**		
	Tet-tuff of Evans Ranch	**Tgp-dac of Guadalupe Pass**	Tcq-quartz latite of Cowboy Rim		
	Tbm-tuff of Black Mountain	Ts-quartz latite of Sycamore Creek	**Tbbc-tuff of Black Bill Canyon**		
	Ta-andesite	Tbg-breccia of Geronimo Pass	Tch-Cedar Hill andesite		
		Tom-dac of Outlaw Mountain	Tw-Walnut Wells monzonite		
		Tsr-rhy of Sloan Ranch	**Tbs-tuff of Bennett Spring**		
		Tbh-breccia of Hog Canyon	Tbb-Bennett Creek breccia		
		Tbu-unnamed biotite-rich tuff	Ta-Animas quartz monzonite		
		Tgc-tuff of Guadalupe Canyon (4)	**Toc-Oak Creek Formation (3)**		
		Tbc-Bluff Creek Formation	**Tbc-Bluff Creek Formation (2)**		
			Ttd-andesite of Taylor Draw		

Notes: Italics indicate units that are divided into members, Bold indicates units dated as part of this study. Numbers in parentheses indicate number of dated samples where greater than one.

Abbreviations: F = flows, B = breccias, P = pyroclastic deposits, rhy = rhyolite, dac = dacite, b/a = basaltic andesite, bas = basalt, porph = porphyry, cong = conglomerate.

calated with numerous local rhyolitic, dacitic, and andesitic lava flows, domes, and dome-related pyroclastic units. The regional ignimbrites have been correlated throughout the area, and provide an integrated stratigraphic framework within which local stratigraphic sequences can be interpreted. The regional ignimbrites are listed in Table 1, which also summarizes age, paleomagnetic polarity, silica content, caldera features, maximum exposed thickness, and volume estimates. The listed ignimbrite-volume estimates are based upon the maximum exposed intracaldera and outflow thicknesses, interpreted cauldron-margin locations, and outflow extents (detailed in McIntosh and Bryan, 2000); these estimates may be in error by as much as a factor of two or three. Table 1 and Figure 4 summarize the $^{40}Ar/^{39}Ar$ from both regional ignimbrites and local units. Figures 2 and 3 depict caldera locations, outflow sheet extents, and sample locations for the major ignimbrites. Figure 5 provides a three-dimensional depiction of the ignimbrite-based time-stratigraphic framework with interlayered, local volcanic units. Table 4 identifies specific correlations between regional ignimbrites and locally named units mapped by previous workers. For some areas, these correlations indicate that revision of existing geologic mapping is needed. The lack of reliable correlation criteria contributed to previous miscorrelation of ignimbrites (Table 4), ultimately causing such problems as spurious proliferation of unit names (e.g. Erb, 1979) and unrecognized fault repeats within stratigraphic sections (e.g., Thorman, 1977).

Outflow facies of two of the nine major ignimbrites, the tuff of Woodhaul Canyon and the tuff of Black Bill Canyon, are very limited in extent. The others are widespread, cropping out in several mountain

TABLE 4. Stratigraphic correlations of regional ignimbrites.

Range:	This study	Peloncillo S	Peloncillo SW	Chiricahua	Peloncillo NW	Peloncillo N	Pyramid N	Pyramid S	Coyote Hills	Animas	Alamo Hurco and Dog	Little Hatchet
Units:	**RC**	Tdc	Tmt	RC								
	PA		Tsc			Taf	Trt7 Trt8	Trt7 Trt8		PA	PA	
	HC		Tbm Trt Tap	HC	Twg Twe Twur Twlr		Trt7	Trt7				
	GI	GI	Tbt Tbm							GI Tgr "BC"	GI Tgr	Tpp
	OC	Tgc						Trt6 Trt5	Tpqw Tpt2	OC Tbc "BC"	OC	
	ST					Tst	Trw	Trt6 Trt5 Trt4 Trt3	Tpt2			
	BC							Trt1	Tr2 Tr1 Tpt1 Tpp Tprt	BC		

Notes: Capitalized abbreviations indicate regional ignimbrites. Boot Heel ignimbrites: RC = Rhyolite Canyon Tuff, PA = Park Tuff, HC = tuff of Horseshoe Canyon, GI = Gillespie Tuff, OC = Oak Creek Tuff, ST = tuff of Steins, BC = Bluff Creek Tuff. Local unit abbreviations and references are given in Table 3. Regional ignimbrite abbreviations in quotation marks indicate miscorrelations by previous workers.

ranges across the field. Source cauldrons have been positively identified for all but one of the nine major ignimbrites, and most of the identified calderas have associated ring-fracture intrusions, moat lavas, or collapse breccias (Table 1). The major ignimbrites can be temporally divided into two groups. Six ignimbrites erupted between 35.2 Ma and 32.7 Ma. After a hiatus of over 5 m.y., the final three ignimbrites erupted in quick succession between 27.6 Ma and 26.8 Ma. The Mogollon-Datil and San Juan volcanic fields to the north experienced similar episodic ignimbrite activity, including similar significant gaps in ignimbrite activity spanning the interval of 32 Ma to 29 Ma (McIntosh et al., 1992b).

Older 35.2–32.7-Ma ignimbrite eruptive pulse

The first eruptive pulse of six ignimbrites began with eruption of the dacitic tuff of Woodhaul Canyon. This ignimbrite has only been identified in the Pyramid Mountains, where the thick, altered exposures have been interpreted as caldera fill (Elston et al., 1978). The age of the sanidine-free reverse-polarity tuff of Woodhaul Canyon is not precisely determined; biotite from a single uncharacteristically fresh sample gave an age of 35.23 ± 0.13 Ma (all errors quoted as ± 2σ) (Table 1, Fig. 4, Appendix 1).

The Bluff Creek Tuff crops out in several of the ranges in the southern half of the volcanic field, but is thickest and most extensive in the Animas Range, in the proposed Tullous caldera (Erb, 1979). It consists of several rhyolitic crystal-poor ignimbrite cooling units, each as much as 200 m thick, with interbedded volcaniclastic conglomerates and sandstones. The tuffs are characteristically lithic-rich, containing clasts of andesite, rare basalt, and rhyolite. Sanidine from four samples of the normal polarity Bluff Creek Tuff yield statistically indistinguishable $^{40}Ar/^{39}Ar$ ages averaging 35.08 ± 0.08 Ma (Table 1, Fig. 4, Appendix 1).

The tuff of Steins forms thick, widespread outcrops in the Peloncillo Mountains north of Steins Pass, where it has been interpreted as caldera fill by Richter et al. (1990). It is normally zoned, from high-silica rhyolite at the base to low-silica rhyolite at the top. Outflow facies crop out throughout the northern ranges of the Boot Heel field (Fig. 3). Eleven dated samples from the tuff of Steins yield an average age of 34.45 ± 0.08 Ma, and the normal polarity of this ignimbrite helps to distinguish it from similar age, reverse polarity, currently uncorrelated ignimbrites in the eastern Boot Heel volcanic field (Table 1, Figs. 4, 5, Appendix 1).

The rhyolitic Oak Creek Tuff forms thick, altered exposures in the Juniper cauldron (Erb, 1979), where is has been intruded by a monzonite resurgent stock. The outflow sheet of this unit is one of the most widespread and distinctive units in the volcanic field. Large, highly fractured, glassy, often pinkish, quartz phenocrysts and large, euhedral hornblende phenocrysts are abundant in this unit. Dinner-plate-sized pumices are common near the base of the unit. The reverse-polarity Oak Creek Tuff is well dated; sanidine from 16 samples average 33.50 ± 0.07 Ma (Table 1, Fig. 4, Appendix 1).

The tuff of Black Bill Canyon is a crystal-rich dacitic tuff of limited distribution. It has only been identified in the Animas Mountains, where thick, potassium-metasomatized exposures have been interpreted as cauldron fill (Erb, 1979). Biotite from one sample of the sanidine-poor, reverse polarity tuff of Black Bill Canyon gave a relatively imprecise age of 33.57 ± 0.18 Ma, within error of the age of the precisely dated 33.50 ± 0.07 Ma Oak Creek Tuff, which stratigraphically underlies the tuff of Black Bill Canyon. Accordingly, the age of the tuff of Black Bill Canyon is rounded down to 33.5 Ma in Table 1.

The youngest regional ignimbrite erupted in the 35.2–32.7 Ma eruptive pulse is the Gillespie Tuff, a normally zoned, low- to high-silica rhyolitic ignimbrite. It crops out extensively in most of the southern

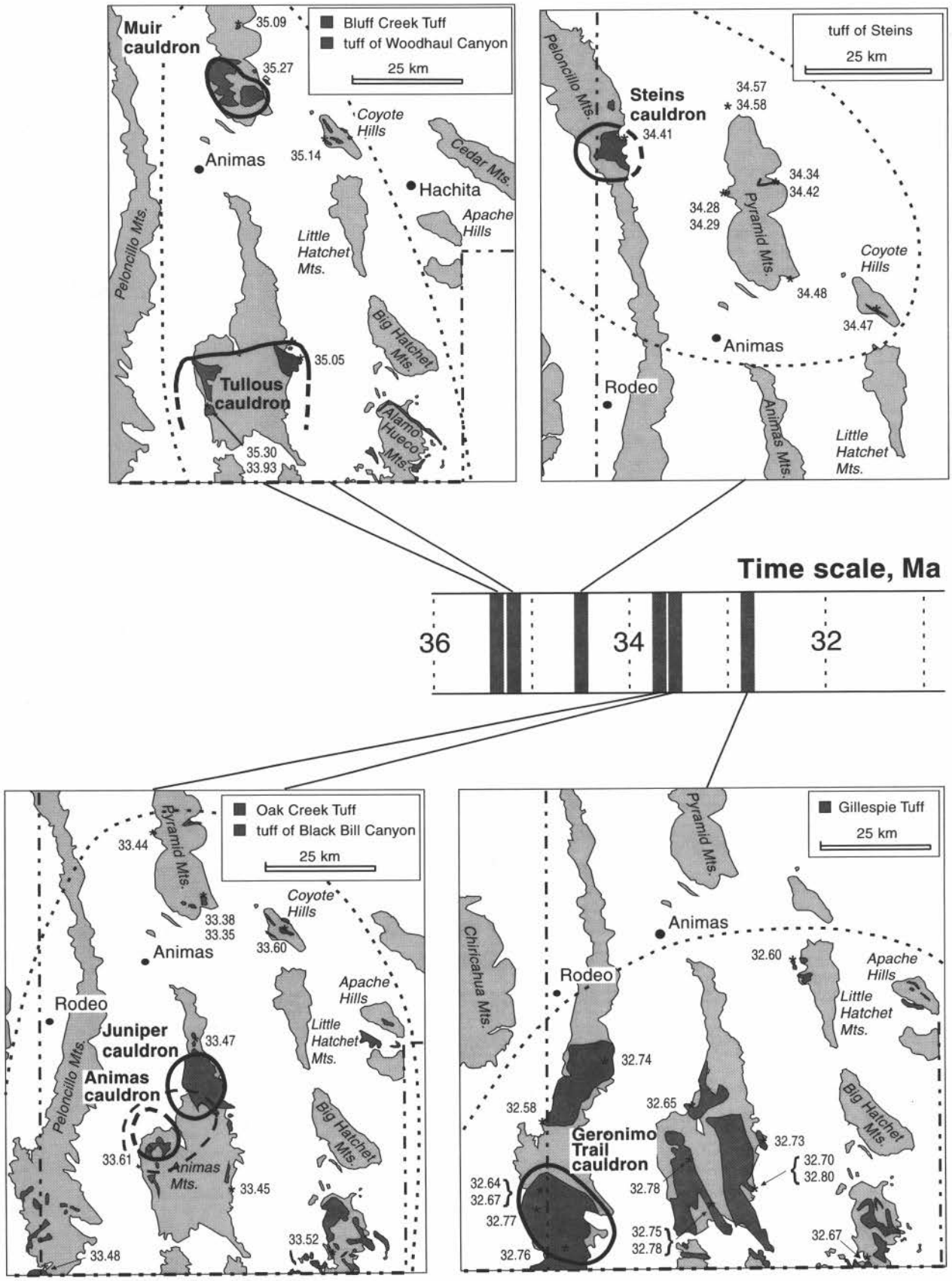

FIGURE 3. Maps showing sample locations, $^{40}Ar/^{39}Ar$ data, outcrop extent, calderas, and approximate minimum outflow sheet area for ignimbrites in the Boot Heel volcanic field. **a**, Older 35.2–32.7-Ma ignimbrites, **b** (facing page), Younger 27.6–26.8-Ma ignimbrites.

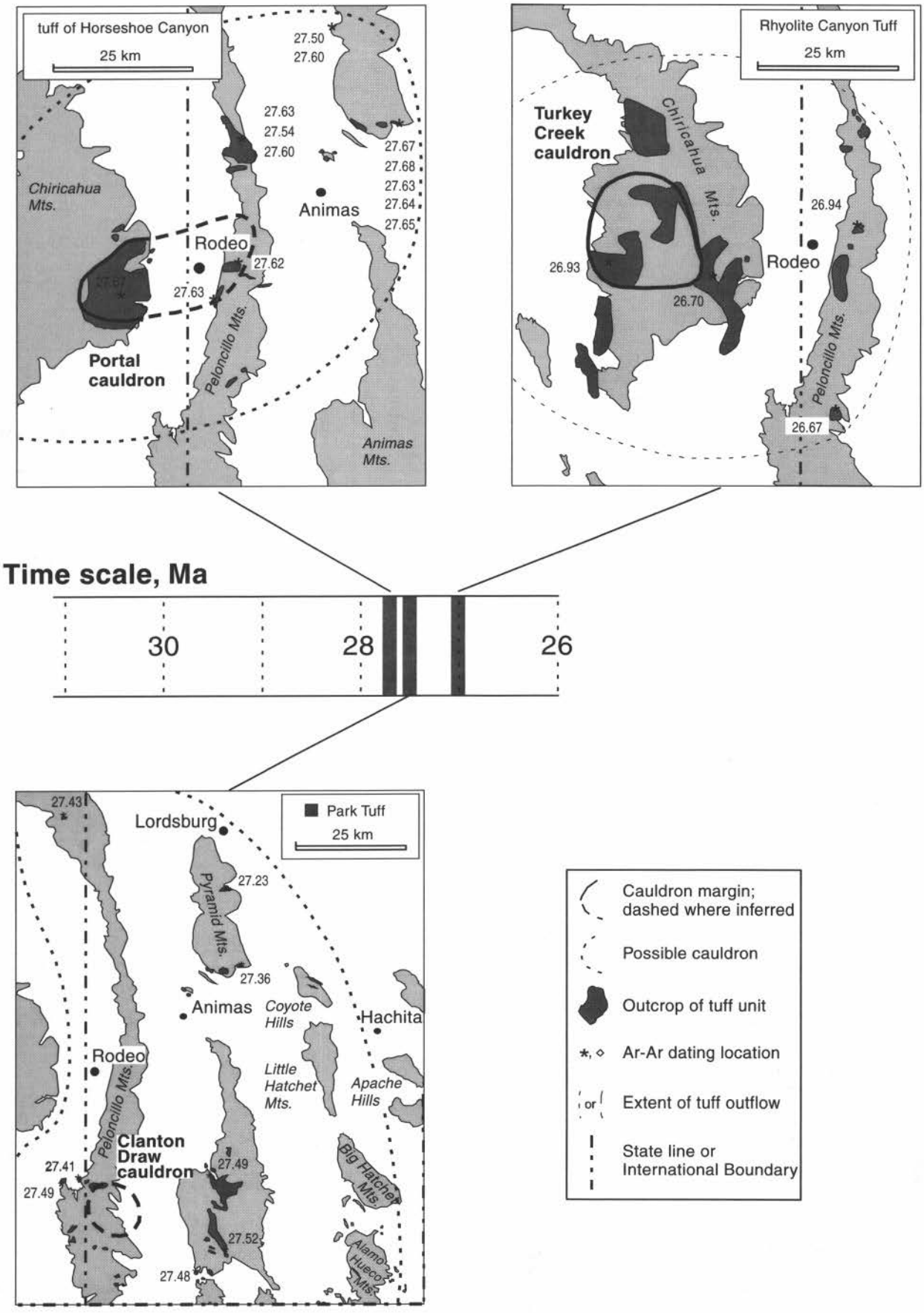
tuff of Horseshoe Canyon
25 km
27.50
27.60
27.63
27.54
27.60
27.67
27.68
27.63
27.64
27.65
Chiricahua Mts.
Animas
Rodeo
27.62
27.63
27.67
Portal cauldron
Peloncillo Mts.
Animas Mts.
Rhyolite Canyon Tuff
25 km
Turkey Creek cauldron
Chiricahua Mts.
26.94
26.93
Rodeo
26.70
Peloncillo Mts.
26.67
Time scale, Ma
30
28
26
Park Tuff
25 km
27.43
Lordsburg
27.23
Pyramid Mts.
27.36
Animas
Coyote Hills
Hachita
Rodeo
Peloncillo Mts.
Little Hatchet Mts.
Apache Hills
Clanton Draw cauldron
27.41
27.49
27.49
Big Hatchet Mts.
27.52
27.48
Alamo Hueco Mts.
Cauldron margin; dashed where inferred
Possible cauldron
Outcrop of tuff unit
Ar-Ar dating location
or
Extent of tuff outflow
State line or International Boundary

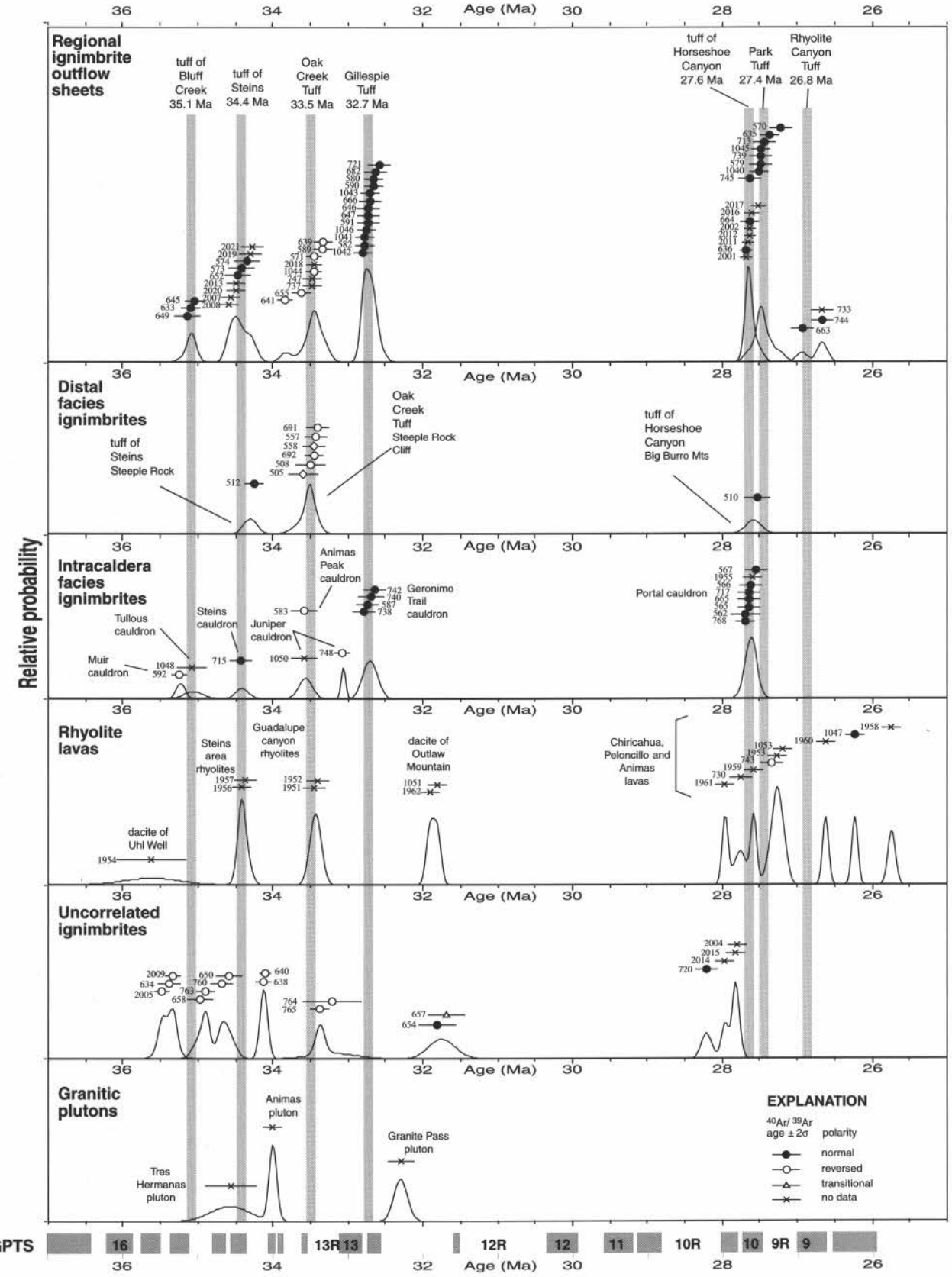

FIGURE 4. Age probability distribution diagram (ideogram) summarizing $^{40}Ar/^{39}Ar$ results from the Boot Heel volcanic field. The age-probability distribution diagram is similar to a histogram but takes into account uncertainties of individual data points. The diagram was constructed using the method of Deino and Potts (1992), by summing the model Gaussian-probability curves for each date. Age data are detailed in Appendix 1 and McIntosh and Bryan (2000). Sources of pluton ages: Tres Hermanas, McLemore (this volume, p. 40); Animas, McLemore et al., 1996; Granite Pass, Channell et al, this volume). Geomagnetic polarity time scale (GPTS) is after McIntosh et al., 1992b.

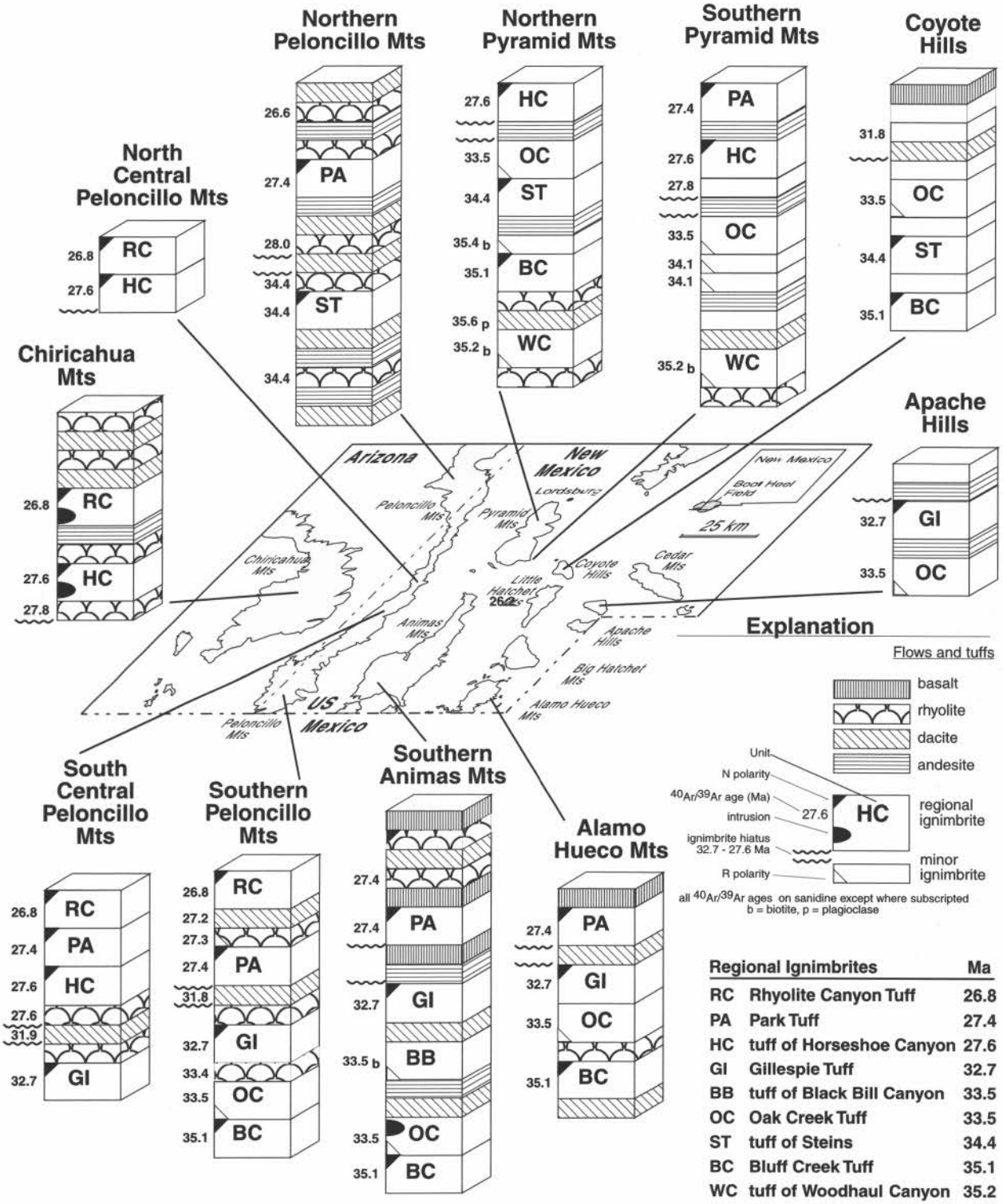

FIGURE 5. Three-dimensional depiction of the ignimbrite-based time-stratigraphic framework for the Boot Heel volcanic field.

mountain ranges in the Boot Heel field. Thick exposures are present in the Animas Mountains and in two locations in the Peloncillo Mountains; all three of these locations have been proposed as potential source calderas for this ignimbrite (Erb, 1979; Elston, 1983, 1984). We consider the Geronimo Trail cauldron (Erb, 1979) in the southern Peloncillo Mountains to be the most likely source for this ignimbrite, primarily because of the well-defined structural margin and extensive associated breccias in this area. A total of 17 dated samples from the normal polarity Gillespie Tuff yield a very precise, weighted mean age of 32.72 ± 0.04 Ma (Table 1, Fig. 4, Appendix 1).

Younger 27.6–26.8-Ma ignimbrite eruptive pulse

Following a 5-m.y. hiatus in ignimbrite activity from 32.7 to 27.6 Ma, a rapid-fire sequence of three ignimbrites was erupted from calderas near the western edge of the Boot Heel volcanic field. All three of these ignimbrites have normal paleomagnetic polarity. The tuff of Horseshoe Canyon forms a thick section in the eastern half of the Chiricahua Mountains, interpreted to be cauldron fill by Bryan (1988, 1995). In this

area, it is strongly zoned, from crystal-poor high-silica rhyolite at the base to crystal-rich dacite at the top. The outflow of the tuff of Horseshoe Canyon is geochemically and petrographically similar to the base of the cauldron fill facies. The outflow sheet crops out in several of the ranges in the western half of the volcanic field (Fig. 3). $^{40}Ar/^{39}Ar$ ages from 17 samples of the tuff of Horseshoe Canyon average 27.63 ± 0.03 Ma (Table 1, Fig. 4, Appendix 1). There is still considerable uncertainty regarding the nature and morphology of the caldera that erupted this ignimbrite. Caldera features of appropriate age extend from the eastern Chiricahua Mountains to the central Peloncillo Mountains (Fig. 3), where multiple ignimbrites are interlayered with volcaniclastic deposits in the Weatherby Canyon area (Drewes and Thorman, 1980b) and caldera-related mesobreccias have been identified in the Antelope Pass area (Edward Deal, 1979, unpublished map).

The second-youngest regional ignimbrite in the Boot Heel field is the Park Tuff, first described by Zeller and Alper (1965) in the Animas Mountains. The Park Tuff crops out as a relatively thin (<75 m) high-silica rhyolite outflow sheet distributed over much of the southern and western volcanic field (Fig. 3). Sanidines from seven samples of the Park Tuff yield an average age of 27.44 ± 0.08 Ma (Table 1, Fig. 4, Appendix 1). No intracaldera facies of the Park Tuff has been identified, but two caldera locations have been proposed. On the basis of ignimbrite flow-direction studies, Erb (1979) proposed a source in the southern Animas Range and adjacent Mexico, termed the San Luis cauldron. On the basis of extensive rhyolitic lavas, McIntyre (1988) proposed the Clanton Draw cauldron in the southern Peloncillo Mountains (Fig. 2). We consider the proposed Clanton Draw cauldron to be the most likely source area for the Park Tuff because Clanton Draw Rhyolite has an appropriate age (27.34 ± 0.14 Ma) and because there is no direct geologic evidence for a caldera in the southern Animas Range.

The youngest regional ignimbrite recognized in the Boot Heel volcanic field is the Rhyolite Canyon Tuff, erupted from the Turkey Creek caldera in the western Chiricahua Mountains (Marjaniemi, 1969; du Bray and Pallister, 1999). The intracaldera facies of the Rhyolite Canyon Tuff is low- to high-silica rhyolite in composition, and is intruded by a dacitic stock. The high-silica rhyolite outflow sheet crops out in several ranges in the western half of the Boot Heel field. Three samples from the Rhyolite Canyon Tuff yielded a weighted mean age of 26.76 ± 0.20 Ma (Table 1, Fig. 4, Appendix 1).

Other activity in the Boot Heel volcanic field

A number of ignimbrites exposed in the Boot Heel volcanic field are relatively thin and locally distributed, and apparently do not correlate with any of the regional ignimbrites discussed above (Figs. 4, 5, Appendix 1). Uncorrelated ignimbrites are most common in the northern and eastern ranges in the volcanic field; suggesting that some may represent distal facies of ignimbrites erupted from the Mogollon-Datil volcanic field. Alternatively, some of the uncorrelated ignimbrites may represent pyroclastic facies of local silicic lava domes.

Rhyolite–dacite lava flows and domes and associated pyroclastic facies are common throughout the Boot Heel field. Many rhyolite lavas are spatially associated with regional ignimbrite calderas. In some cases (e.g., tuff of Steins, Fig. 5), intracaldera-facies ignimbrites are both underlain and overlain by rhyolite lavas of almost identical age; these are interpreted as precursor activity preceding catastrophic caldera eruptions followed by post-caldera moat fill activity. Rhyolite-lava volcanism was particularly widespread and voluminous during the 27.6–26.8-Ma pulse of ignimbrite volcanism (Fig. 4, Appendix 1). Rhyolite lavas in this age interval are exposed in the Chiricahua Mountains, in the Animas Range, and in the Peloncillo Mountains at Clanton Draw in the south and Doubtful Canyon in the north. McIntosh et al. (1992a) noted that voluminous rhyolite lavas were also associated with the final pulse in the Mogollon-Datil volcanic field. They suggested that local crustal, tectonic conditions might have allowed magmas to degas prior to eruption. The abundance of lavas within the younger eruptive pulse in the Boot Heel field may likewise reflect local crustal, tectonic conditions. Alternatively, the abundance of younger lavas may reflect lower volatile contents of younger magmas, as discussed below. In addition to silicic extrusive rocks, a small number of mid-Cenozoic granitic to dioritic plutons and stocks are exposed in the Boot Heel volcanic field (Fig. 5). Some of these intrude recognized cauldron sequences and others are distant from known calderas. Available $^{40}Ar/^{39}Ar$ data from these silicic intrusive bodies (Fig. 5) indicate that most were emplaced during the older 35.2–32.7-Ma pulse of ignimbrite volcanism.

Volcanic sequences in the Boot Heel volcanic field commonly include some intermediate to mafic lavas in addition to the abundant dacitic-to-rhyolitic ignimbrites and lavas (Fig. 5). Because they lack sanidine, precise ages cannot be obtained from most of these intermediate to mafic lavas, although some precise age constraints are provided by stratigraphically bracketing silicic units (Fig. 5). All of the numerous intermediate and mafic lavas are of relatively local distribution and were probably erupted predominantly by stratovolcanos. Although no attempt was made to quantitatively assess the erupted volume of intermediate and mafic lavas, they are clearly volumetrically subordinate to the silicic ignimbrites and lavas. This low ratio of less-silicic to more-silicic volcanic rocks is similar to the low ratio observed in the Mogollon-Datil volcanic field (McIntosh et al., 1992a), but contrasts with the much higher proportion of andesites in the San Juan volcanic field (Lipman et al., 1978).

GEOCHEMISTRY AND PETROGENESIS OF THE BOOT HEEL VOLCANIC FIELD

In the Boot Heel volcanic field, the abundance of high-precision $^{40}Ar/^{39}Ar$ age data allow us to resolve temporal chemical variations in the ignimbrites, with confidence in the ages and stratigraphic relationships of the units. In addition, the proximity of the relatively well-characterized Mogollon-Datil volcanic field allows us to examine and contrast the possible effects of crustal thickness and extension on melt chemistry and/or eruptive style.

Geochemical sampling was concentrated on the regional ignimbrites. These account for most of the volume of the rocks erupted and are commonly zoned, necessitating the collection of multiple samples to characterize the unit fully. Also, most of the available $^{40}Ar/^{39}Ar$ data from the Boot Heel field are from the regional ignimbrites. In addition to the ignimbrites, samples were collected from the abundant rhyolitic and dacitic lava flows, and less abundant andesitic and basaltic lavas. Also sampled were a few cauldron-related intrusions, including resurgent stocks and ring-fracture dikes. Sample localities (Fig. 3) are detailed in Bryan (1995) and McIntosh and Bryan (2000).

Major- and trace-element chemistry

The ignimbrites of the mid-Tertiary Boot Heel volcanic field are rhyolitic–trachydacitic in composition, using the IUGS classification scheme (Fig. 6) of Le Bas et al. (1986). Lava flows, domes, and intrusions have more variable compositions. Rhyolites and trachydacites are most abundant. Less common are basalts, basaltic andesites, andesites, and trachyandesites (termed "latites" in many field studies, e.g., Bryan, 1995).

Volcanic rocks of the older and younger eruptive pulses described above are chemically distinct. This distinction is most apparent in the nine major ignimbrites. Although ignimbrites from both eruptive pulses are zoned (Table 1), maximum SiO_2 contents are higher for younger ignimbrites. For a given silica content, the three ignimbrites of the 27.6–26.8-Ma pulse are relatively enriched in MnO, K_2O, TiO_2, and Na_2O, and depleted in CaO, MgO, and P_2O_5 (Fig. 7), relative to the six ignimbrites of the older 35.2–32.7-Ma pulse. Relative to the older units, the younger ignimbrites are also uniformly enriched in the Large-Ion Lithophile (LIL) elements, the High-Field Strength (HFS) elements, and the Rare-Earth Elements (REE), except for Eu. The systematic differences in HFS element concentrations between the older and younger pulses is readily apparent on a plot of Zr/TiO_2 versus Zr (Fig. 8). The Zr/TiO_2 ratio varies systematically between the older ignimbrites (Zr/TiO_2 is ~500) and the younger ignimbrites (Zr/TiO_2 > 800). Trace elements variations are less pronounced between younger and older intermediate-composition lavas (Figure 8 and Bryan, 1995).

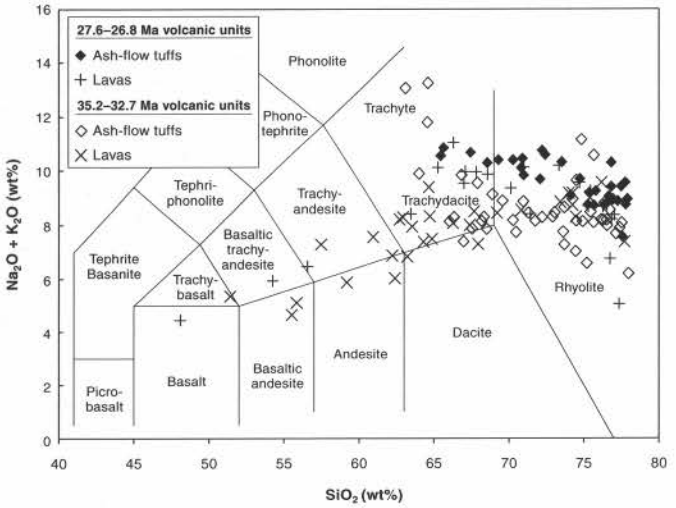

FIGURE 6. The classification of volcanic rocks of the Boot Heel volcanic field using the IUGS classification scheme of Le Bas et al. (1986).

Trace-element compositional trends within zoned ignimbrites also vary between the young and old pulses (Fig. 7). In general, trace-element depletion and enrichment trends tend to be steeper in zoned ignimbrites of the younger pulse, compared to those of the older pulse (Bryan, 1995). For example, Ba and Eu exhibit strong depletions with increasing silica content in the younger ignimbrites, and vary much less in the zoned ignimbrites of the older pulse. In Figure 7, this results in a crossing pattern; the dacitic end members of the younger ignimbrites are enriched in Ba and Eu relative to the dacitic older tuffs, whereas the rhyolitic end members are strongly depleted relative to similar-composition tuffs in the older pulse.

The steep trace-element enrichment and depletion trends within the younger 27.6–26.8-Ma zoned ignimbrites indicate that they underwent more fractionation than the older ignimbrites. The strong depletion of Sr, Ba, Eu, Zr, and Hf, and moderate depletion of light REE in felsic portions of younger zoned ignimbrites indicate that feldspar and zircon were important fractionating phases. This is consistent with the modal mineral compositions of the felsic portions of younger ignimbrites, which is quartz and sanidine ± plagioclase ± biotite, with zircon as a trace mineral constituent.

Trace-element-concentration trends within older 35.2–32.7-Ma ignimbrites indicate that ferromagnesian minerals were important fractionating phases. The heavy REE and and the HFS elements Nb, Y, and Ta are either depleted or show no enrichment with silica content in the older ignimbrites (Bryan, 1995). Fractionation of ferromagnesian phases is consistent with the modal mineral compositions of the older ignimbrite, which commonly contain biotite, hornblende, and clinopyroxene.

Isotope chemistry

Isotopic analyses (Table 5) do not reveal any major systematic differences between the younger 27.6–26.8-Ma and older 35.2–32.7-Ma eruptive pulses of the Boot Heel volcanic field (Table 3; complete isotope data is in Bryan (1995) and McIntosh and Bryan (2000)). The $(^{87}Sr/^{86}Sr)_o$ values for rocks of both pulses fall within the same range, from 0.708 to 0.714, with the exception of the Oak Creek Tuff, which has initial ratios between 0.714 and 0.716. Pb isotopes for both groups of rocks are identical. The younger 27.6–26.8-Ma volcanic units have $(^{143}Nd/^{144}Nd)_o$ ratios approximately 1.5 ε_{Nd} units more positive than the older 35.2–32.7-Ma units. $\varepsilon_{Nd(o)}$ values for the younger ignimbrites and lavas average -5.68, while those of the older units average -7.34.

The Nd, Sr, and Pb isotopic compositions of Boot Heel volcanic field rocks suggest that the source magmas are mixtures of mantle-derived basaltic magmas and a Precambrian crustal component. Nd isotopes suggest that the younger magmas contain a somewhat larger mantle component that those of the older pulse, but Pb and Sr isotopes do not reflect this. One unexpected pattern in the $^{87}Sr/^{86}Sr$ initial ratios is a consistent trend within each ignimbrite unit towards lower $(^{87}/_{86})_o$ with increasing SiO_2 (or decreasing Sr content). This trend is unusual.

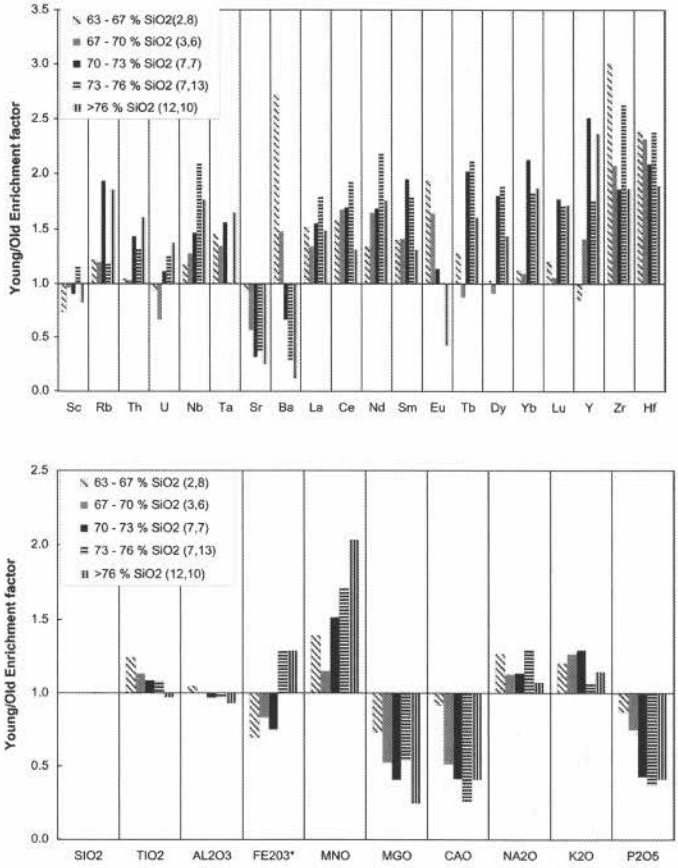

FIGURE 7. Elemental enrichment factors for younger 27.6–26.8-Ma ignimbrites relative to older 35.2–32.7-Ma ignimbrites of the same silica content. The young/old "enrichment factors" are the average composition of the younger ignimbrites in each range divided by that of the older ignimbrites. Enrichment factors are >1 if the younger ignimbrites are enriched relative to the older ignimbrites, <1 if they are depleted relative to the older ignimbrites. Silica ranges are given in the legend, followed in parentheses by the number of ignimbrite samples in the younger and older groups, respectively.

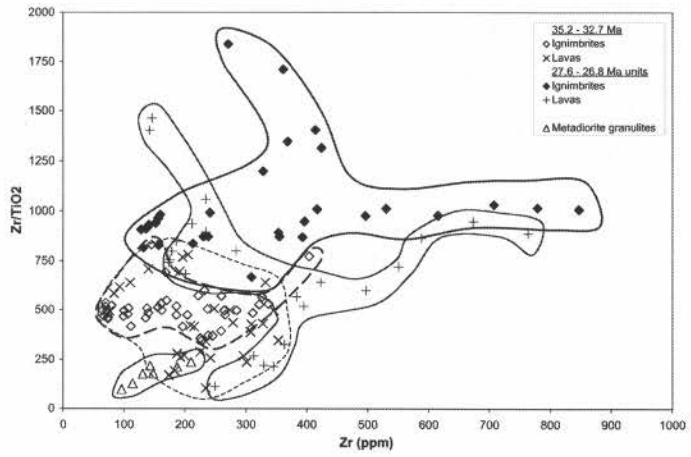

FIGURE 8. Zr/TiO_2 ratios of ignimbrites and lavas in the Boot Heel volcanic field. Also shown for comparison are ratios from meta-diorite xenoliths from the Geronimo volcanic field (Kempton et al., 1990).

TABLE 5. Sr, Nd, and Pb isotopic compositions of units in the Boot Heel field.

Sample	Age (Ma)	$(^{87}Sr/^{86}Sr)_i$	$(^{143}Nd/^{144}Nd)_i$	$(^{206}Pb/^{204}Pb)_i$	$(^{207}Pb/^{204}Pb)_i$	$(^{208}Pb/^{204}Pb)_i$
1	26.8	0.71043	0.512361	18.605	15.590	39.101
2	27.4	0.70497	0.512304	18.515	15.590	38.904
3	27.6	0.71001	0.512251	18.525	15.628	38.937
4	27.6	0.71340	0.512291	18.516	15.582	38.964
5	32.7	0.70824	0.512213	18.564	15.588	39.003
6	32.7	0.71271	0.512216	18.530	15.577	38.929
7	33.5	0.71067	0.512153	18.335	15.555	38.792
8	33.5	0.71538	0.512241	18.444	15.596	38.934
9	34.4	0.70760	0.512214	18.633	15.610	39.030
10	34.4	0.71191	0.512197	18.646	15.592	38.978
11	35.1	0.71079	0.512233	18.392	15.571	38.649
12	35.2	0.71080	0.512279	18.620	15.658	39.303
13	~26.9	0.70850	0.512351	18.200	15.561	38.740
14	~26.9	0.70962	0.512309	18.527	15.584	38.978

Notes: $(^{143}Nd/^{144}Nd)i$ ratio corrected for fractionation using $(^{146}Nd/^{144}Nd) = 0.721900$

Analyzed samples:

1 Rhyolite Canyon Tuff (BH-4)
2 Park Tuff (BH-8)
3 tuff of Horseshoe Can., rhyolite base (BH-27)
4 tuff of Horseshoe Can., dacite top (BH-17)
5 Gillespie Tuff, high-silica rhyolite base (BH-41)
6 Gillespie Tuff, rhyolite top (BH-39)
7 tuff of Black Bill Canyon (BH-54)
8 Oak Creek Tuff (BH-62)
9 tuff of Steins, high-silica rhyolite base (BH-73)
10 tuff of Steins, rhyolite top (BH-77)
11 Bluff Creek Tuff (BH-81)
12 tuff of Woodhaul Canyon (BH-86)
13 basaltic andesite, Chiricahua Mts (BH-136)
14 monzonite stock, Turkey Creek cauldron (BH-93)

Isotope variations in the silicic volcanic rocks of the Sierra Madre and Mogollon-Datil volcanic fields (Abitz, 1989; Seaman, 1988; Duffield and Ruiz, 1992) follow the opposite trend, where $^{87}Sr/^{86}Sr$ initial ratios increase with SiO_2 content. There are a number of possible explanations for this unusual trend. In some cases (for example, samples from the Animas Peak area), variation in the initial Sr ratios is due at least in part to Rb introduction during potassium metasomatism. However, given the chemical evidence that the high-silica rhyolitic and dacitic parts of individual zoned ignimbrites are cogenetic, it seems probable that the variation in Sr_i is primarily due to contamination of the ignimbrite source magmas either before or during eruption. Possible contaminants include Phanerozoic sedimentary rocks and andesitic magma.

Contamination of silicic magmas by Phanerozoic sedimentary rocks, especially limestone, is considered likely because the Boot Heel field is located at the northern end of the Pedregosa basin, where the carbonate-rich sedimentary section was initially several kilometers thick and may have been further thickened by Laramide-age thrust faulting. Boot Heel source magmas may have been contaminated by assimilation of wall rocks or stoped blocks, or by fluid exchange between stoped blocks and the magma. If carbonate sediments are the main source of contamination, this may explain why similar Sr_i trends are not seen in the Sierra Madre or Mogollon-Datil volcanic fields. The thick Pedregosa basin section is only present in extreme southwestern New Mexico, southeastern Arizona, and northern Mexico.

Mixing of silicic and andesitic magmas during eruption of zoned magma chambers is indicated by abundant andesitic-magma clots in some of the ignimbrites. Further evidence for magma mixing during the cauldron-forming eruptions is seen in disequilibrium textures and trace element trends of post-cauldron dacitic lavas (Bryan, 1995). Syn-eruptive mixing of magmas with different crustal assimilation histories may have contributed the unusual Sr_i patterns observed in the Boot Heel volcanic field.

Petrogenesis

Trace-element modeling, together with isotopic data, suggests that geochemical variations within Boot Heel ignimbrites and lavas are primarily due to crystal fractionation (Bryan, 1995). Based on the evidence summarized below, we conclude that the best explanation for the systematic geochemical differences between the younger and older volcanic pulses is that the source magmas for younger pulse were less volatile-rich:

(1) Isotopic compositions of Boot Heel volcanic field rocks suggest that source magmas were derived from isotopically similar mixtures of mantle-derived basaltic magmas and subordinate amounts of assimilated crustal components. Nd isotopes suggest that the younger magmas contain a slightly larger mantle component than those of the older pulse, but Pb and Sr isotopes do not reflect this.
(2) Hydrous phases, primarily hornblende and biotite, are much more abundant in older volcanic units (Bryan, 1995; McIntosh and Bryan, 2000).
(3) Trace-element-enrichment trends within zoned ignimbrites suggest that fractionation of amphibole was much more important in source magmas for the older units, probably because of their higher water contents (Bryan, 1995).
(4) The volume ratio of silicic lavas to ignimbrites is much higher for the younger eruptive pulse, possibly because magmas of the older eruptive pulse were more volatile-rich, and less likely to erupt passively as lavas.
(5) Steep trace-element-variation trends within younger zoned ignimbrites indicate that higher degrees of fractionation occurred prior to their eruption, relative to fractionation during the older pulse (Fig. 7). This is consistent with relatively H_2O-poor magmas, where volatile contents did not become high enough to support ash-flow eruptions until the fraction of remaining melt was small.
(6) Tectonic discrimination diagrams (Pearce et al., 1984) indicate that units of the older eruptive pulse plot in subduction-related fields, or are transitional between subduction-related and within-plate fields (Fig. 9). Most of the younger volcanic rocks plot in within-plate fields. The Pearce et al. (1984) discrimination diagrams are based upon the behavior of the HFS elements, which are depleted in hydrous volcanic arc magmas.

We do not completely understand the process by which younger source magma in the Boot Heel field became progressively drier, although we consider it to be a consequence of the mid-Cenozoic progressive transition from subduction to extensional tectonic conditions in southwestern North America. Subduction-related magmas are generally more hydrous than within-plate magmas, because of dehydration and volatile loss from the subducted plate (Pearce et al., 1984). Fractional crystallization of hydrous phases such as amphibole and biotite are responsible for the HFS element depletions characteristic of volcanic arc magmas and seen in older Boot Heel ignimbrites. In addition, it is possible that amphibole or other hydrous phases were present in the crustal components of Boot Heel magmas and acted as stable restite phases during the older eruptive pulse, perhaps because of the presence of H_2O-rich fluids rising from the subducted plate. In the case of the younger, drier pulse, hydrous phases may no longer have been stable in the restite assemblage, breaking down to produce anhydrous assemblages such as ilmenite, pyroxenes, and plagioclase. Because the bulk K_d values of most trace elements for these anhydrous assemblages are

FIGURE 9. Tectonic discrimination diagrams from Pearce et al. (1984). Fields are WPG = within-plate granites; ORG = ocean ridge granites; VAG = volcanic arc granites; COLG = collisional granites.

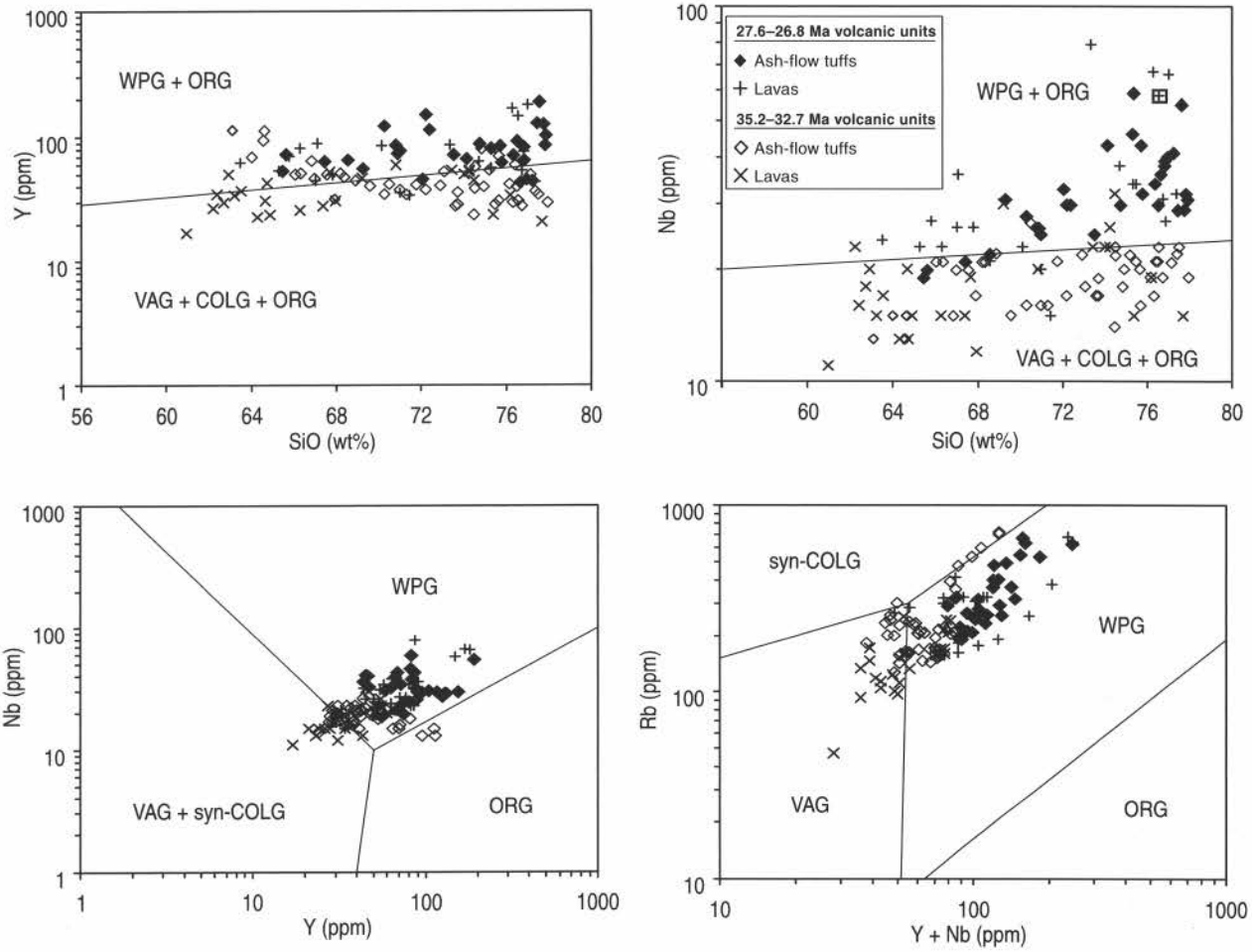

low, resulting partial melts would have been relatively enriched in trace elements, especially the HFS elements.

TECTONIC SIGNIFICANCE OF BOOT HEEL VOLCANISM

Numerous workers (e.g., Atwater, 1970; Lipman et al., 1972, 1978; Elston, 1976; Livacarri, 1979; Cross and Pilger, 1982) have suggested that systematic changes in Cretaceous–Cenozoic volcanism and tectonism in southwestern North America were caused by plate tectonic events along the western margin of the North American plate. In broad terms, Laramide compression and andesitic volcanism are interpreted as consequences of an episode of anomalous low-angle subduction of the Farallon plate (Cross and Pilger, 1982). Beginning at about 35 Ma, the spreading ridge of the Farallon plate first contacted the North American plate (Atwater, 1970; Severinghouse and Atwater, 1990), which ultimately caused a subduction-to-extension transition that began in Colorado, New Mexico, and west Texas and swept westward into the Great Basin. Although many workers agree on the general nature of this transition, there are a wide variety of interpretations of the timing, details, mechanisms, and consequences of the process. It is clear that the transition process spanned at least several million years. Some recent studies (e.g., Perry et al., 1987, 1988) have focused on the difference between pre-20-Ma and post-20-Ma volcanic rocks. This change from voluminous calc-alkaline suites to less-voluminous bimodal suites has been ascribed to an increase in asthenosphere-derived magmas and a corresponding decrease in lithosphere-derived magmas. Other workers have also noted distinct but less dramatic geochemical changes in pre-30-Ma versus post-30-Ma mafic–silicic rocks in southwestern North America (e.g., Davis and Hawkesworth, 1993, 1994, 1995).

Geochemical trends in ignimbrites of the Boot Heel suggest that progressive lowering of volatile contents of source magmas between 32.7 and 27.6 Ma may have had a significant effect on fractional crystallization processes during differentiation of silicic magma bodies. Exhaustion of slab-derived volatiles or dehydration of the lithospheric mantle may have played a part in this process.

The strongly episodic and regionally synchronous timing of caldera volcanism in the Boot Heel and adjacent silicic volcanic fields also has implications for the nature of the mid-Cenozoic North American subduction-to-extension transition. Boot Heel ignimbrites erupted in two brief pulses (35.2-32.7 Ma) and (27.6-26.8 Ma), separated by a 5.1 m.y.-long hiatus in caldera eruptions. The Mogollon-Datil, San Juan, and Thirtynine Mile volcanic fields to the north experienced similar episodic ignimbrite activity, including similar significant gaps in ignimbrite activity spanning 32–29 Ma (McIntosh et al., 1992b). The synchronized nature and brevity of caldera-forming eruptive pulses in these volcanic fields, which together range over a distance of 1000 km, suggests that the regional state of stress may have played a key role in initiating or suppressing caldera volcanism. Regionally synchronized changes in crustal stress contrast strongly with the time-transgressive nature of the transition from subduction to transform movement that has occurred along the western margin of north America, which began approximately 35 Ma and continues to this day (Atwater, 1970: Severinghouse and Atwater, 1990). Further refinements in the chronology of mid-Cenozoic volcanism in the western United States and less-studied western Mexico will help our understanding of the relationship between episodic, abrupt, regionally synchronized subduction-to-extension processes within the north American plate, and the more continuous, regionally time-transgressive subduction-to-transform transition processes along the plate

margin.

SUMMARY AND CONCLUSIONS

High-precision $^{40}Ar/^{39}Ar$ geochronology, paleomagnetic analyses, and geochemical studies of regional ignimbrites have helped define a time-stratigraphic framework for the late Eocene–Oligocene Boot Heel volcanic field of southwestern New Mexico. Single-crystal and bulk $^{40}Ar/^{39}Ar$ dating results provide precise (± 0.25–0.5%) ages for sanidine-bearing rhyolite–rhyodacite ignimbrites and lavas, and somewhat less-precise age determinations for biotite or plagioclase from less silicic sanidine-free units. Paleomagnetic polarity and direction, together with geochemical analyses, help refine regional correlations based on $^{40}Ar/^{39}$ data.

Nine large-volume ignimbrites in the Boot Heel volcanic field erupted in two distinct pulses (35.2–32.7 Ma and 27.6–26.8 Ma) separated by a 5.1-m.y. hiatus in ignimbrite activity (Table 1). Source calderas are recognized for eight of the ignimbrites, and seven of the ignimbrites include widespread regional outflow facies. Caldera activity shifted from east to west during the life span of the volcanic field. Local volcanic units intercalated with the regional ignimbrites include basaltic, andesitic, dacitic, and rhyolitic flows and pyroclastic rocks. Some of these units are associated with regional ignimbrite calderas.

The two ignimbrite pulses exhibit distinctive petrologic and chemical differences. The 35.2–32.7 Ma activity occurred in the early phases of the mid-Cenozoic subduction-to-extension transition along the western coast of North America. Volatile flux through the upper mantle and crust was high due to dehydration reactions in the subducted plate. Amphibole is a common, phenocryst phase in the older ignimbrites, and was probably an important cumulate phase in the more-mafic source magmas. The 27.6–26.8 Ma pulse occurred later in the subduction-to-extension transition, and the source magmas were relatively H_2O-poor. Amphibole was no longer part of the fractionating assemblage, leading to comparative enrichment in those elements that are strongly partitioned into hornblende (e.g., the high-field-strength elements). The younger magmas had longer crustal-residence times, undergoing greater degrees of crystal fractionation before volatile concentrations reached levels able to support effusive pyroclastic eruptions. Many of the younger rhyolitic magmas erupted passively, as lavas. Hence, the younger ignimbrites tend to be low- to high-silica rhyolite in composition, whereas the older ignimbrites are dacitic-to-rhyolitic. Trace element concentrations reflect these differences. Younger ignimbrites have steep enrichment and depletion patterns, whereas older units have relatively flat trends. Neodymium, Sr, and Pb isotopic compositions of the volcanic rocks indicate that source magmas were mixtures of mantle-derived basaltic magmas and Precambrian crust. Compositional differences between the two age groups are primarily due to changes in fractionating crystal assemblages rather than changes in the composition or relative proportion of mantle and crustal melt components.

ACKNOWLEDGMENTS

This work was supported in part by the New Mexico Bureau of Mines, the University of New Mexico, Sandia National Laboratory, and by National Science Foundation Grant EAR-8903417. Mick Kunk and John Sutter of the U.S. Geological Survey generously provided access to their laboratory for initial resistance-furnace $^{40}Ar/^{39}Ar$ analyses. Access to geochemical analytical facilities was provided by Los Alamos National Laboratory and the Oregon State Reactor-Sharing Program (INAA), Doug Brookins at the UNM Geochronology Laboratory (Rb-Sr), and Doug Walker and Jon Lynn at the Kansas Geochronology Laboratory (Sm-Nd and Pb). We offer special thanks to Wolf Elston for his contributions to this research. We thank landowners in the Boot Heel of New Mexico for generous access to private land. This manuscript was improved by reviews from Virginia McLemore and Steve Cather.

REFERENCES

Abitz, R. J., 1989, Geology and petrogenesis of the northern Emory caldera, Sierra County, New Mexico [Ph.D. dissertation]: Albuquerque, University of New Mexico, 174 p.

Armstrong, A. K., Silberman, M. L., Todd, V. R., Hoggatt, W. C. and Carter, R. B., 1978, Geology of the central Peloncillo Mountains, Hidalgo County, New Mexico: New Mexico Bureau of Mines and Mineral Resources, Circular 158, 19 p.

Atwater, T., 1970, Implications of plate tectonics for the Cenozoic tectonic evolution of western North America: Geological Society of America Bulletin, v. 81, p. 3513–3535.

Severinghouse, J. and Atwater, T., 1990, Cenozoic geometry and thermal store of the subduring slabs beneath western North America: Geological Sciety of American Bulletin, v. 176, p. 1–22.

Bryan, C. R., 1988, Geology and geochemistry of mid-Tertiary volcanic rocks in the eastern Chiricahua Mountains, southeastern Arizona [M.S. thesis]: Albuquerque, University of New Mexico, 137 p.

Bryan, C. R., 1989, Geologic map and sections of the Cochise Head quadrangle and adjacent areas, southeastern Arizona: New Mexico Bureau of Mines and Mineral Resources, Memoir 46, p. 153–157.

Bryan, C. R., 1995, Stratigraphy, chemistry, and petrogenesis of volcanic rocks of the mid-Tertiary Boot Heel volcanic field, southwestern New Mexico, and southeastern Arizona [Ph.D. dissertation]: Albuquerque, University of New Mexico, 272 p.

Cross, T. A. and Pilger, R. H., 1982, Controls on subduction geometry, location of magmatic areas, and tectonics of arc and back-arc regions: Geological Society of America Bulletin, v. 93, p. 545–562.

Davis, J. and Hawkesworth, C., 1993, The petrogenesis of 30–20 Ma basic and intermediate volcanics from the Mogollon-Datil volcanic field, New Mexico, USA: Contributions to Mineralogy and Petrology, v. 115, p. 165–183.

Davis, J. and Hawkesworth, C. J., 1994, Early calc-alkaline magmatism in the Mogollon-Datil volcanic field, New-Mexico, USA: Journal of the Geological Society, v. 151, p. 825–843.

Davis, J. M. and Hawkesworth, C. J., 1995, Geochemical and tectonic transitions in the evolution of the Mogollon-Datil volcanic field, New Mexico, USA: Chemical Geology, v. 119, p. 31–53.

Deal, E. G., Elston, W. E., Erb, E. E., Peterson, S. L., Reiter, D. E., Damon, P. E. and Shafiqullah, M., 1978, Cenozoic volcanic geology of the Basin-and-Range province in Hidalgo County, New Mexico: New Mexico Geological Society, Guidebook 29, p. 219–229.

Deino, A. and Potts, R., 1990, Single-crystal $^{40}Ar/^{39}Ar$ dating of the Olorgesailie Formation, southern Kenya rift: Journal of Geophysical Research, v. 95, p. 8453–8470.

Deino, A. and Potts, R., 1992, Age-probability spectra for examination of single-crystal $^{40}Ar/^{39}Ar$ dating results: examples from Olorgesailie, southern Kenya rift: Quaternary International, v. 13/14, p. 47–53.

Drewes, H., 1982, Geologic map and sections of the Cochise Head quadrangle and adjacent areas, southeastern Arizona: U.S. Geological Survey, Miscellaneous Investigations Series Map I-1686, scale 1:24,000.

Drewes, H., 1986, Geologic map of the northern part of the Animas Mountains, Hidalgo County, New Mexico: U.S. Geological Survey, Miscellaneous Investigations Series Map I-1686, scale 1:24,000.

Drewes, H. and Thorman, C. H, 1980a, Geologic map of the Steins quadrangle and the adjacent part of the Vanar quadrangle, Hidalgo County, New Mexico: U.S. Geological Survey, Miscellaneous Investigations Series Map I-1220, scale 1:24,000.

Drewes, H. and Thorman, C. H., 1980b, Geologic Map of the Cotton City quadrangle and the adjacent part of the Vanar quadrangle, Hidalgo County, New Mexico: U.S. Geological Survey, Miscellaneous Investigations Series Map I-1221, scale 1:24,000.

Drewes, H. and Williams, F. E., 1973, Mineral resources of the Chiricahua Wilderness Area, Cochise County, Arizona: U.S. Geological Survey, Bulletin 1385-A, 53 p.

du Bray, E. A. and Pallister, J. S., 1994a, Geologic map of the Chiricahua Peak quadrangle, Cochise County, Arizona: U.S. Geological Survey, Map GQ-1733, scale 1:24,000.

du Bray, E. A. and Pallister, J. S., 1994b, Geologic map of the Stanford Canyon quadrangle, Cochise County, Arizona: U.S. Geological Survey Map, GQ-1743, 1:24,000.

du Bray, E. A. and Pallister, J. S, 1999, Recrystallization and anatexis along the plutonic-volcanic contact of the Turkey Creek caldera, Arizona: Geological Society of America Bulletin, v. 111, p. 143–153.

Duffield, W. A. and Ruiz, J., 1992, Compositional gradients in large reservoirs of silicic magma as evidenced by ignimbrites versus Taylor Creek Rhyolite lava domes: Contributions to Mineralogy and Petrology, v. 110, p. 190–210.

Elston, W. E., 1976, Tectonic significance of mid-Tertiary volcanism in the Basin and Range province: a critical review with special reference to New Mexico:

New Mexico Geological Society, Special Publication 5, p. 93–102.
Elston, W. E., 1983, Cenozoic volcanic centers in the New Mexico segment of the Pedregosa basin—constraints on oil and gas exploration in southwestern New Mexico: New Mexico Energy Research and Development Institute, Report 2-66-1304, 54 p.
Elston, W. E., 1984, Mid-Tertiary ash-flow tuff cauldrons, southwestern New Mexico: Journal of Geophysical Research, v. 89, p. 8733–8750.
Elston, W. E., Deal, E. G. and Logsdon, M. J., 1978, Geology and geothermal waters of the Lightning Dock Region, Animas Valley and Pyramid Mountains, Hidalgo County, New Mexico: New Mexico Bureau of Mines and Mineral Resources, Circular 177, 44 p.
Enlows, H. E., 1951, The igneous geology of Chiricahua National Monument, Arizona: Tulsa Geological Society Digest, v. XIX, p. 105–107.
Enlows, H. E., 1955, Welded tuffs of the Chiricahua National Monument, Arizona: Geological Society of America Bulletin, v. 66, p. 1215–1246.
Erb, E. E., 1979, Petrologic and structural evolution of ash-flow tuff cauldrons and noncauldron-related volcanic rocks in the Animas and southern Peloncillo Mountains, Hidalgo County, New Mexico [Ph.D. dissertation]: Albuquerque, University of New Mexico, 286 p.
Fernandez, L. A., Jr., and Enlows, H. F., 1966, Petrography of the Faraway Ranch Formation, Chiricahua National Monument, Arizona: Geological Society of America Bulletin, v. 77, p. 1017–1030.
Finnell T., 1987, Geologic map of the Cliff quadrangle, Grant County, New Mexico: U.S. Geological Survey, Miscellaneous Investigation Series Map I-1768, scale 1:50,000.
Flege, R. F., 1959, Geology of the Lordsburg quadrangle, Hidalgo County, New Mexico: New Mexico Bureau of Mines and Mineral Resources, Bulletin 62, 36 p.
Gebben, D. J., 1979, Geology of the central Peloncillo Mountains, the northern third of the Pratt quadrangle, Hidalgo County, New Mexico [M.S. thesis]: Kalamazoo, Western Michigan University, 127 p.
Gillerman, E., 1958, Geology of the central Peloncillo Mountains, Hidalgo County, New Mexico, and Cochise County, Arizona: New Mexico Bureau of Mines and Mineral Resources, Bulletin 57, 152 p.
Hayes, P. T., 1982, Geologic map of the Buck Robinson Peak and Whitmire Canyon Roadless Areas, Coronado National Forest, New Mexico and Arizona: U.S. Geological Survey, Miscellaneous Field Studies Map MF-1425-A, scale 1:62,500.
Hedlund, D. C., 1978, Geologic map of the C Bar Ranch Quadrangle, Grant and Hidalgo Counties, New Mexico: U.S. Geological Survey, Miscellaneous Field Map MF-1039, scale 1:24,000.
Hedlund, D. C., 1990, Geologic map and sections of the Steeple Rock quadrangle, Grant and Hidalgo Counties, New Mexico: U.S. Geological Survey, Open-file Report 90-240, 14 p.
Henry, C. D., Kunk, M. J. and McIntosh, W. C., 1994, $^{40}Ar/^{39}Ar$ chronology and volcanology of silicic volcanism in the Davis Mountains, Trans-Pecos Texas; with Supplemental Data 9442: Geological Society of America Bulletin, v. 106, p. 1359–1376.
Hildreth, W. and Mahood, W., 1985, Correlation of ash-flow tuffs: Geological Society of America Bulletin, v. 96, p. 968–974.
Hudson, J. S., 1984, Geology and hydrothermal alteration of the San Simon mining district south of Steins Pass, Peloncillo Mountains, Hidalgo County, New Mexico [M.S. thesis]: Albuquerque, University of New Mexico, 125 p.
Kempton, P. D., Harmon, R.S., Hawkesworth, C.J. and Moorbath, S., 1990, Petrology and geochemistry of lower crustal granulites from the Geronimo volcanic field, southeastern Arizona: Geochimica et Cosmochimica Acta, v. 54, p. 3401–3426.
Lasky, S. G., 1938, Geology and ore deposits of the Lordsburg Mining District, Hidalgo County, New Mexico: U.S. Geological Survey, Bulletin 885, 62 p.
Lasky, S. G., 1947, Geology and ore deposits of the Little Hatchet Mountains, Hidalgo and Grant Counties, New Mexico: U.S. Geological Survey, Professional Paper 208, 101 p.
Latta, J. S., 1983, Geochemistry and petrology of the ash flows of Chiricahua National Monument, Arizona, and their relation to the Turkey Creek caldera [M.S. thesis]: Tucson, University of Arizona, 194 p.
Le Bas, M. J., LeMaitre, R.W., Streckheisen, A. and Zanettin, B., 1986, A chemical classification of volcanic rocks based on the total alkali-silica diagram: Journal of Petrology, v. 27, p. 745–750.
Lipman, P. W., Doe, B. R., Hedge, C. E. and Steven, T. A., 1978, Petrologic evolution of the San Juan volcanic field, southwestern Colorado, Pb and Sr isotopic evidence: Geological Society of America Bulletin, v. 89, p. 59–82.
Lipman, P. W., Protska, H. J. and Christianson, R. L., 1972, Cenozoic volcanism and plate tectonic evolution of the western United States; I. Early and Middle Cenozoic: Royal Society of London Philosophical Transactions, Series A, v. 272, p. 217–248.
Livaccari, R. F., 1979, Late Cenozoic tectonic evolution of the western United States: Geology, v. 7, p. 72–75.
Marjaniemi, D. K., 1969, Geologic history of an ash-flow sequence and its source area in the Basin-and-Range Province of southeastern Arizona [Ph.D. dissertation]: Tucson, University of Arizona, 263 p.
Marvin, R. F. and Dobson, S.W., 1979, Radiometric ages—compilation B; U.S. Geological Survey: Isochron/West, v. 26, p. 3–32.
Marvin, R. F., Naeser, C.W. and Mehnert, H.H., 1978, Tabulation of radiometric ages—including unpublished K-Ar and fission track—for rocks in southeastern Arizona and southwestern New Mexico: New Mexico Geological Society, Guidebook 29, p. 243–252.
McIntosh, W. C., 1991, Evaluation of paleomagnetism as a correlation criterion for Mogollon-Datil ignimbrites, southwestern New Mexico: Journal of Geophysical Research, v. 96, p. 13,459–13,483.
McIntosh, W. C. and Bryan, C.R., 2000, $^{40}Ar/^{39}Ar$, paleomagnetic, and geochemical data from the Boot Heel volcanic field, New Mexico: New Mexico Bureau of Mines and Mineral Resources, Open-file Report OF-AR-12, 36 p.
McIntosh, W. C. and Chamberlin, R. M., 1994, $^{40}Ar/^{39}Ar$ geochronology of middle to late Cenozoic ignimbrites, mafic lavas, and volcaniclastic rocks in the Quemado region, New Mexico: New Mexico Geological Society, Guidebook 45, p. 165–185.
McIntosh, W. C., Chapin, C. E., Ratté, J. C. and Sutter, J. F., 1992a, Time-stratigraphic framework for the Eocene–Oligocene Mogollon-Datil volcanic field, southwest New Mexico: Geological Society of America Bulletin, v. 104, p. 851–871.
McIntosh, W. C., Geissman, J. W., Chapin, C. E., Kunk, M. J. and Henry, C. D., 1992b, Calibration of the latest Eocene–Oligocene geomagnetic polarity time scale using $^{40}Ar/^{39}Ar$ dated ignimbrites: Geology, v. 20, p. 459–463.
McIntosh, W. C., Sutter, J. F., Chapin, C. E. and Kedzie, L. L., 1990, High-precision $^{40}Ar/^{39}Ar$ sanidine geochronology of ignimbrites in the Mogollon-Datil volcanic field, southwestern New Mexico: Bulletin of Volcanology, v. 52, p. 584–601.
McIntyre, D. H., 1988, Volcanic geology in parts of the southern Peloncillo Mountains, Arizona and New Mexico: U.S. Geological Survey, Bulletin 1671, 18 p.
McLemore, V. T., McIntosh, W. C. and Pease, T. C., 1996, $^{40}Ar/^{39}Ar$ age determinations of four plutons associated with mineral deposits in southwestern New Mexico: New Mexico Bureau of Mines and Mineral Resource, Open-file Report OF-410, 36 p.
Pallister, J. S. and du Bray, E.A., 1994, Geologic map of the Fife Peak quadrangle, Cochise County, Arizona: U.S. Geological Survey, Map GQ-1708, scale 1:24,000.
Pallister, J. S. and du Bray, E.A., 1989, Field guide to volcanic and plutonic features of the Turkey Creek caldera, Chiricahua Mountains, southeast Arizona: New Mexico Bureau of Mines and Mineral Resources, Memoir 46, p. 138–152.
Pallister, J. S., du Bray, E. A. and Latta, J. S., IV, 1994, Geologic map of the Rustler Park quadrangle, Cochise County, Arizona: U.S. Geological Survey, Map GQ-1696, scale 1:24,000.
Pearce, J. A., Harris, N. B. W. and Tindle, A. G., 1984, Trace element discrimination diagrams for the tectonic interpretation of granitic rocks: Journal of Petrology, v. 25, p. 956–983.
Perry, F. V., Baldridge, W. S. and Depaolo, D. J., 1987, Role of asthenosphere and lithosphere in the genesis of late Cenozoic basaltic rocks from the Rio Grande rift and adjacent regions of the southwestern United States: Journal of Geophysical Research, Solid Earth and Planets, v. 92, p. 9193–9213.
Perry, F. V., Baldridge, W. S. and Depaolo, D. J., 1988, Chemical and isotopic evidence for lithospheric thinning beneath the Rio Grande rift: Nature, v. 332, p. 432–434.
Peterson, S. L., 1976, Geology of the Apache No. 2 mining district, Hidalgo County, New Mexico [M.S. thesis]: Albuquerque, University of New Mexico, 86 p.
Raydon, G. T., 1952, Geology of the northwestern Chiricahua Mountains, Arizona [M.S. thesis]: Berkeley, University of California Berkeley, 52 p.
Reiter, D. E., 1980, Geology of the Alamo Hueco and Dog Mountains, Hidalgo County, New Mexico [M.S. thesis]: Albuquerque, University of New Mexico, 99 p.
Richter, D. H., Lawrence, V. A., Drewes, H., Young, T. H., Enders, M. S., Damon, P. E. and Thorman, C. H., 1990, Geologic map of the San Simon quadrangle and parts of the Summit Hills and Mondel quadrangles, Cochise, Graham, and Greenlee Counties, Arizona, and Hidalgo County, New Mexico: U.S. Geological Survey, Miscellaneous Investigations Series Map I-1951, scale 1:24,000.
Sabins, F. F., Jr., 1957, Geology of the Cochise Head and western part of the Vanar quadrangles, Arizona,: Geological Society of America Bulletin, v. 68, p.

1315–1342.
Seager, W. R. and Clemons, R. E., 1988, Geology of Hermanas quadrangle, Lunca County, New Mexico: New Mexico Bureau of Mines and Mineral Resources, Geologic Map 63, scale 1:24,000.
Seaman, S. J., 1988, Geology and petrogenesis of ash-flow tuffs and rhyolitic magmas associated with the Gila Cliff Dwellings basin–Bursum caldera complex, southwestern New Mexico, [Ph.D. dissertation]: Albuquerque, University of New Mexico, 170 p.
Smith, F. C., 1987, Geology, mineralization and exploration potential of the McGhee Peak area, San Simon mining district, Hidalgo County, New Mexico [M.S. thesis]: Albuquerque, University of New Mexico, 176 p.
Strongin, O., 1958, Geology and ore deposits of the Apache Hills and northern Sierra Rica, Hidalgo County, New Mexico [Ph.D. dissertation]: New York, Columbia University, 222 p.
Thorman, C. H., 1977, Geologic map of the Coyote Peak and Brockman quadrangles, Hidalgo and Grant counties, New Mexico: U.S. Geological Survey, Miscellaneous Field Studies Map MF-924, scale 1:24,000.
Thorman, C. H. and Drewes, H., 1978, Geologic map of the Gary and Lordsburg quadrangles, Hidalgo County, New Mexico: U.S. Geological Survey, Miscellaneous Investigations Series Map I1151, scale 1:24,000.
Thorman, C. and Drewers, H., 1981, Geologic map of the Gage SW quadrangle, Grant and Luna Counties, New Mexico: U.S. Geological Survey, Miscellaneous Investigation Series Map I-1231, scale 1:24,000.
Wrucke, C. T. and Bromfield, C. S., 1961, Reconnaissance geologic map of part of the southern Peloncillo Mountains, Hidalgo County, New Mexico: U.S. Geological Survey, Mineral Investigations Field Studies Map MF-160, scale 1:62,500.
Zeller, R. A., Jr., 1958, Reconnaissance geology of Dog Mountains quadrangle: New Mexico Bureau of Mines and Mineral Resources, Geologic Map 8, scale 1:62,500.
Zeller, R. A., Jr., 1962, Reconnaissance geologic map of southern Animas Mountains: New Mexico Bureau of Mines and Mineral Resources, Geologic Map 17, scale 1:62,500.
Zeller, R. A., Jr., 1970, Geology of the Little Hatchet Mountains, Hidalgo and Grant Counties, New Mexico: New Mexico Bureau of Mines and Mineral Resources, Bulletin 96, 23 p.
Zeller, R. A., Jr., and Alper, A.M., 1965, Geology of the Walnut Wells quadrangle, Hidalgo County, New Mexico: New Mexico Bureau of Mines and Mineral Resources, Bulletin 84, 105 p.

APPENDIX— $^{40}Ar/^{39}Ar$ AGES, PALEOMAGNETIC DATA, AND SAMPLE LOCATIONS

						Paleomagnetic data				$^{40}Ar/^{39}Ar$ data					
Sample	Map Unit	Range	Lat (°N)	Long (°W)	Facies	Polarity	Inclination	Declination	α95	Mineral	Analysis	K/Ca	±2σ	Age	±2σ
Rhyolite Canyon Tuff - 26.8 Ma															
663	Tmt	Peloncillo SW	31.803	108.934	O	N	61.6	350.7	5.7	san	F	30.8		26.94	0.14
733	RC	Chiricahua	31.772	109.197	O					san	F	30.3		26.66	0.14
744	Tdc	Peloncillo S	31.578	109.005	O	N	56.8	335.1	1.5	san	F	33.1		26.67	0.14
Park Tuff - 27.4 Ma															
570	Trt7	Pyramid	32.221	108.691	O	N	66.2	8.4	2.2	san	F	28.5		27.23	0.14
579	PA	Animas	31.616	108.736	O	N	53.6	337.7	1.2	san	F	16.4		27.49	0.14
635	Trt8	Pyramid	32.061	108.642	O	N	40.8	328.7	6.1	san	F	-		27.36	0.12
713	Taf	Peloncillo N	32.398	109.113	O	N	75.5	350.7	3.7	san	F	32.6		27.43	0.14
739	Tsc	Peloncillo SW	31.444	109.122	O	N	61.2	55.9	2.8	san	F	30.8		27.49	0.14
745	Tsc	Peloncillo SW	31.587	109.026	O	N	63.4	348.0	1.8	san	F	23.4		27.64	0.14
1040	PA	Animas	31.396	108.765	O	N	58.3	336.0	2.9	san	L	30.1	7.2	27.50	0.12
1045	PA	Animas	31.441	108.706	O	N	51.1	353.9	5.1	san	L	26.1	16.3	27.48	0.08
581	PA	Animas	31.575	108.713	O	N	60.6	334.0	1.5						
588	PA	Alamo Hueco	31.402	108.399	O	N	54.4	344.5	8.1						
tuff of Horsehoe Canyon 27.6 Ma															
562	HC	Chiricahua	31.786	109.179	C	N	43.1	48.8	5.4	san	L	17.5		27.67	0.22
565	Tbm	Peloncillo SW	31.777	108.997	C	N	36.5	2.6	9.0	san	F	19.8		27.63	0.14
566	Twg	Peloncillo NW	32.010	108.943	C	N	41.0	46.8	5.2	san	F	20.4		27.60	0.14
567	Twe	Peloncillo NW	32.014	108.943	C	N	34.0	49.0	3.1	san	F	22.7		27.54	0.14
636	Trt7	Pyramid	32.061	108.646	O	N	33.8	29.2	5.2	san	F	-		27.67	0.10
637	Trt7	Pyramid	32.061	108.649	O	N	42.8	30.9	2.3						
664	Trt	Peloncillo SW	31.827	108.948	O	N	88.3	317.5	4.4	san	F	16.8		27.62	0.14
717	Twe	Peloncillo NW	32.010	108.957	C	N	29.7	47.9	2.4	san	F	19.1		27.63	0.14
564	Tbm	Peloncillo SW	31.783	108.998	C	N	44.0	359.7	2.7						
732	HC	Chiricahua	31.771	109.197	C	N	53.8	329.5	1.7						
734	HC	Chiricahua	31.770	109.205	C	N	14.8	0.5	3.1						
1955	Tfql	Chiricahua	31.816	109.232	C					san	L	19.0	14.0	27.58	0.08
2001	Trt7	Pyramid	32.064	108.665	O					san	L	28.1	4.9	27.68	0.09
2002	Trt7	Pyramid	32.063	108.664	O					san	L	28.9	6.3	27.63	0.08
2017	Trt7	Pyramid	32.212	108.802	O					san	L	29.7	6.5	27.50	0.13
2016	Trt7	Pyramid	32.212	108.802	O					san	L	29.9	4.1	27.60	0.09
2012	Trt7	Pyramid	32.064	108.665	O					san	L	28.0	6.2	27.64	0.08
2011	Trt7	Pyramid	32.063	108.663	O					san	L	29.1	4.4	27.65	0.07
665	Tap	Peloncillo SW	31.829	108.948	C	N	63.9	63.6	32.5	san	F	32.5		27.63	0.14
768	Twlr	Peloncillo NW	32.001	108.949	C	N	43.7	37.0	3.5	san	L	23.7	4.9	27.67	0.10
568	Twur	Peloncillo NW	32.021	108.926	C	N	60.1	349.3	7.6						
766	Twur	Peloncillo NW	32.020	108.926	C	N	45.1	213.5	30.7						
716	Twh	Peloncillo NW	32.009	108.966	C	N	34.9	356.7	4.0						
569	Twlr	Peloncillo NW	32.001	108.970	C	N	54.0	347.5	4.1						
767	Twlr	Peloncillo NW	32.000	108.948	C	N	57.1	68.4	2.9						
510	Twtd	Big Burro	32.476	108.443	X	N	64.0	5.7	3.3	san	F	31.4		27.58	0.20
Gillespie Tuff - 32.7 Ma															
580	Gl	Animas	31.564	108.719	O	N	34.5	353.7	1.8	san	F	-		32.65	0.10
582	Gl	Animas	31.580	108.803	O	N	4.8	344.4	3.6	san	F	-		32.78	0.10
587	Tgc?	Peloncillo S	31.484	109.086	C	N	14.9	10.0	5.8	san	F	68.5		32.73	0.16
590	Tgr	Alamo Hueco	31.392	108.386	O	N	35.7	351.9	6.6	san	F	-		32.65	0.10
591	Gl	Alamo Hueco	31.393	108.387	O	N	24.0	345.0	4.3	san	F	72.1		32.73	0.16
646	Gl	Animas	31.581	108.602	O	N	58.4	335.1	5.3	san	F	76.9		32.73	0.16
647	Gl	Animas	31.578	108.599	O	N	32.8	347.6	3.5	san	F	73.5		32.73	0.16
666	Tbm	Peloncillo SW	31.738	108.890	O	N	46.0	351.7	4.8	san	F	70.2		32.71	0.16

						Paleomagnetic data				$^{40}Ar/^{39}Ar$ data					
Sample	Map Unit	Range	Lat (°N)	Long (°W)	Facies	Polarity	Inclination	Declination	α95	Mineral	Analysis	K/Ca	±2σ	Age	±2σ
Gillespie Tuff - 32.7 Ma (cont.)															
680	Tpp	Little Hatchet	31.901	108.505	O	N	21.7	333.4	5.1						
681	Tpp	Little Hatchet	31.901	108.504	O	N	44.4	326.9	4.9						
682	Tpp	Little Hatchet	31.901	108.504	O	N	50.1	329.6	6.0	san	F	70.4		32.62	0.16
719	Tbt	Peloncillo SW	31.621	109.056	O	N	24.5	339.1	6.1						
721	Tbt	Peloncillo SW	31.610	109.037	O	N	17.8	11.8	2.8	san	F	70.1		32.58	0.16
735	Tgc	Peloncillo S	31.367	109.027	O	N	36.0	351.2	1.7						
738	Tgc	Peloncillo S	31.446	109.060	C	N	59.3	347.8	3.3	san	F	65.1		32.77	0.16
740	Tgc	Peloncillo S	31.486	109.079	C	N	19.1	4.3	1.8	san	F	57.2		32.67	0.18
742	Tgc	Peloncillo S	31.489	109.070	C	N	26.0	358.3	13.0	san	F	71.2		32.64	0.16
1041	GI	Animas	31.395	108.770	O	N	2.4	335.1	3.8	san	L	58.8	9.4	32.78	0.09
1042	BC	Animas	31.506	108.620	O	N	48.4	359.3	4.4	san	L	70.4	11.1	32.79	0.09
1043	GI	Animas	31.506	108.621	O	N	32.1	349.2	5.0	san	L	69.9	12.2	32.70	0.09
1046	GI	Animas	31.441	108.706	O	N	18.6	349.4	1.3	san	L	64.8	14.3	32.76	0.10
tuff of Black Bill Canyon - <33.5 Ma (biotite = 33.61 Ma)															
583	BB	Animas	31.581	108.804	C	R	-39.7	180.6	4.1	bio	L	83.8	105.9	33.57	0.18
584	BB	Animas	31.579	108.813	C	R	-46.5	184.3	2.8						
643	BB	Animas	31.657	186.609	O	R	-35.8	187.5	3.9						
644	BB	Animas	31.629	108.585	C	R	-24.9	186.0	7.6						
Oak Creek Tuff - 33.5 Ma															
571	Trt6	Pyramid	32.219	108.694	O	R	-54.9	189.9	8.0	san	F	52.6		33.44	0.16
589	OC	Alamo Hueco	31.392	108.388	O	R	-46.3	173.4	7.0	san	F	52.2		33.32	0.16
639	Trt6	Pyramid	32.059	108.662	O	R	-47.2	157.7	5.0	san	F	53.6		33.32	0.16
641	Trt5	Pyramid	32.058	108.659	O	R	-45.7	157.5	3.3	san	F	-		33.83	0.14
629	Trt5	Pyramid	32.223	108.718	O	R	-54.2	161.8	4.6						
631	Trt5	Pyramid	32.219	108.726	O	R	-51.5	175.5	2.6						
653	Tpt2	Coyote Hills	32.010	108.495	O	R	-43.2	149.6	2.7						
642	OC	Animas	31.657	108.610	O	R	-59.2	184.7	4.3						
655	Tpqw	Coyote Hills	32.011	108.496	O	R	-44.6	170.6	3.0	san	F	53.3		33.61	0.16
747	OC	Animas	31.786	108.713	O					san	F	54.7		33.47	0.18
748	OC	Animas	31.712	108.687	C						F			33.06	0.06
737	Tgc	Peloncillo S	31.343	109.073	O					san	F	54.0		33.48	0.16
1044	BC	Animas	31.505	108.618	O	R	-54.6	174.2	4.2	san	L	51.8	3.2	33.45	0.09
1050	BC	Animas	31.499	108.787	C					san	L	11.7	2	33.56	0.18
628	Trt6	Pyramid	32.222	108.719	O	R	-62.8	155.8	2.5						
632	Trt6	Pyramid	32.219	108.726	O	R	-59.3	154.0	2.2						
656	Tpqw	Coyote Hills	32.010	108.480	O	R	-57.5	125.8	3.4						
662	Tpqw	Coyote Hills	32.026	108.471	O	R	-53.6	164.8	2.8						
2018	Trt6	Pyramid	32.212	108.801	O					san	L	52.0	4.3	33.44	0.13
505	Tmc	Cliff	32.841	108.597	O					san	F	22.6		33.65	0.24
508	Tk	Big Burro	32.500	108.478	O	R	-54.7	101.4	3.3	san	F	54.2		33.55	0.24
557	Tcc	Cliff	32.873	108.694	O	R	-48.0	174.4	2.0	san	F	29.0		33.48	0.16
558	Tfcc	Cliff	32.855	108.702	O	N	41.0	350.1	8.6	san	F	23.9		33.51	0.16
691	Ttm8	Steeple Rock	32.756	108.879	O	R	-60.6	148.6	2.0	san	F	55.3		33.46	0.16
692	Ttm5	Steeple Rock	32.751	108.882	O	R	-51.4	167.5	3.7	san	F	55.9		33.51	0.16
tuff of Steins 34.4 Ma															
715	ST	Peloncillo N	32.355	109.022	C	N	48.6	29.7	1.9	san	F	56.9		34.41	0.18
652	Tpt2	Coyote Hills	32.010	108.496	O	N	71.6	32.6	5.5	san	F	66.2		34.47	0.18
573	Trt4	Pyramid	32.216	108.697	O	N	58.1	38.7	2.3	san	F	52.1		34.42	0.18
574	Trt3	Pyramid	32.215	108.697	O	N	56.1	42.2	5.3	san	F	64.7		34.34	0.18
714	ST	Peloncillo N	32.297	108.988	O	N	29.6	19.3	2.2						
572	Trt4	Pyramid	32.217	108.697	O	N	53.4	41.0	2.2						
630	Trt4	Pyramid	32.220	108.726	O	N	55.8	35.3	5.2						
2021	Trt4	Pyramid	32.212	108.800	O					san	L	56.7	36.7	34.28	0.17
2019	Trt5	Pyramid	32.212	108.800	O					san	L	49.3	21.7	34.29	0.16
2013	Trt6	Pyramid	32.063	108.666	O					san	L	19.2	12.8	34.48	0.11
2020	Trt4	Pyramid	32.212	108.800	O					san	L	50.3	32.3	34.48	0.12
2007	Trw	Pyramid N	32.351	108.792	O					san	L	35.7	27.1	34.57	0.12
2008	Trw	Pyramid N	32.351	108.792	O					san	L	50.4	54.4	34.58	0.11
512	Tam	Steeple Rock	32.777	108.942	O	N	50.8	26.7	4.7	san	F	51.5		34.30	0.18
Bluff Creek Tuff - 35.1 Ma															
645	BC	Animas	31.612	108.581	O	N	41.9	343.0	12.9	san	F	-		35.05	0.12
1048	BC	Animas	31.499	108.789	C					san	L	20.9	56.2	35.06	0.25
633	Trt1	Pyramid	32.223	108.730	O	N	57.6	341.9	3.4	san	F	-		35.09	0.10
649	Tpp	Coyote Hills	32.006	108.495	O	N	59.2	338.4	4.3	san	F	24.6		35.14	0.18
585	BC	Animas	31.570	108.813	C	N	66.6	290.5	5.4						
586	BC	Animas	31.571	108.813	C										
651	Tpt1	Coyote Hills	32.007	108.495	O	N	66.2	354.6	2.7						
659	Tr2	Coyote Hills	32.031	108.468	O	N	59.8	333.2	4.2						
660	Tr1	Coyote Hills	32.030	108.470	O	N	58.8	276.5	3.2						
648	Tprt	Coyote Hills	32.000	108.493	O	N	46.8	21.8	20.1	san	F	94.3		36.78	0.18
tuff of Woodhaul Canyon - 35.2 (biotite)															
592	WC	Pyramid	32.113	108.666	C	R	-58.4	172.1	3.3	bio	L	124.9	126.0	35.23	0.13

						Paleomagnetic data				$^{40}Ar/^{39}Ar$ data					
Sample	Map Unit	Range	Lat (°N)	Long (°W)	Facies	Polarity	Inclination	Declination	α95	Mineral	Analysis	K/Ca	±2σ	Age	±2σ
Rhyolite lavas, intrusives, and breccias															
1047	Tpt	Animas	31.384	108.780	L	N	46.2	12.5	1.7	san	L	19.2	9.6	26.23	0.08
1053	Tda	Peloncillo S	31.442	108.903	L					san	L	10.3	2.5	27.19	0.11
743	Tcd	Peloncillo S	31.518	109.018	L	R	-59.8	173.7	7.9	san	F	35.0		27.34	0.14
563	Tldp	Chiracahua	31.776	109.132	L	R	-3.0	344.7	1.9						
730	Tcc	Chiricahua	31.883	109.174	L					san	F	19.9		27.76	0.16
1051	Tom	Peloncillo S	31.512	109.040	L					san	L	48.6	38.2	31.81	0.10
1958	Tocl	Peloncillo S	31.773	109.002	L					san	L	38.0	12.6	25.74	0.11
1960	Thrr	Peloncillo N	32.412	109.066	L					san	L	44.3	16.2	26.62	0.08
1953	Tpc	Animas	31.578	108.729	L					san	L	16.3	4.5	27.27	0.10
1959	Tocl	Peloncillo S	31.775	108.999	L					san	L	16.2	6.9	27.58	0.08
1961	Tmd	Peloncillo N	32.354	109.148	L					san	L	10.1	1.9	27.96	0.09
1962	Tom	Peloncillo SW	31.592	109.063	L					san	L	56.9	34.5	31.91	0.10
1952	Twg	Peloncillo S	31.353	109.047	L					san	L	14.2	21.3	33.40	0.14
1951	Tgc	Peloncillo S	31.340	109.079	L					san	L	17.3	33.6	33.46	0.14
1957	Tsr	Peloncillo N	32.365	109.054	L					san	L	68.9	231.0	34.38	0.16
1956	Trr	Peloncillo N	32.308	108.976	L					san	L	22.7	24.3	34.42	0.10
1954	Tu	Pyramid	32.173	108.744	L					plag	L	0.1	0.1	35.62	0.75
741	Thc	Peloncillo S	31.476	109.094	B	R?	-34.8	82.7	38.7	san	F	51.1		33.34	0.18
Uncorrelated Tuffs, including Rimrock/Coyote/ Carrizalillo/Cedar Mts. tuffs															
2004	Trt6	Pyramid	32.063	108.663	M					san	L	21.9	10.3	27.80	0.10
2015	Trt6	Pyramid	32.061	108.662	M					san	L	21.1	6.0	27.83	0.08
2014	Trt6	Pyramid	32.062	108.662	M					san	L	21.4	7.0	27.96	0.11
746	Tsc	Peloncillo SW	31.590	109.026	M	N	62.8	353.9	2.9						
720	Tws	Peloncillo SW	31.605	109.029	M	N	66.8	352.8	7.4	san	F	102.7		28.21	0.14
736	Tgc	Peloncillo S	31.343	109.073	M	R	-47.9	138.7	2.9						
769	Tet	Peloncillo SW	31.934	108.924	M	N	24.7	357.1	8.0						
770	Tbt	Peloncillo SW	31.917	108.916	M	R	-14.2	96.7	56.3						
1052	Twc	Peloncillo SW	31.524	109.050	M										
654	Tplt	Coyote Hills	32.015	108.496	X	T	15.1	147.5	3.8	san	F	54.0		31.80	0.16
657	Tplt	Coyote Hills	32.012	108.480	X	N	54.7	336.1	10.7	san	F	2.8		31.69	0.18
661	Tplt	Coyote Hills	32.027	108.470	X	T	7.8	146.3	6.1						
765	Tr	Cedar Mts	32.003	108.223	U	R	-51.8	148.7	6.9	san	L	50.6	6.3	33.37	0.12
764	Tr	Cedar Mts	32.008	108.227	U	R	-9.7	149.6	53.9	san	L	25.0	10.5	33.20	0.61
640	Trt4	Pyramid	32.057	108.661	M	R	-38.9	167.6	6.1	san	F			34.11	0.10
638	Trt4	Pyramid	32.056	108.660	M	R	-16.0	150.8	2.4	san	F			34.13	0.10
650	Tptw	Coyote Hills	32.008	108.494	M	R	-31.0	189.8	3.4	san	F	63.7		34.58	0.18
658	Tr3	Coyote Hills	32.032	108.467	M	R	-23.8	172.0	5.8	san	F	46.3		34.98	0.18
760	Tj	Carrizalillo Hills	31.870	107.973	M	R	-26.5	170.5	2.3	san	L	42.9	5.6	34.68	0.13
634	Trt2	Pyramid	32.223	108.728	M	R	-58.3	164.6	4.0	bio	L	370.2	359.8	35.39	0.24
2009	Tr	Pyramid N	32.345	108.809	M					san	L	21.8	10.8	35.33	0.11
2005	Tr	Pyramid N	32.346	108.798	M					san	L	17.0	16.0	35.47	0.12
761	Tc	Carrizalillo Hills	31.819	107.933	U										
762	Tc	Carrizalillo Hills	31.819	107.933	U	T	-8.1	288.0	51.2						
763	Tc	Carrizalillo Hills	31.804	107.924	U	R	-42.0	147.2	2.7	san	L	46.2	2.7	34.89	0.09
Potentially correlative units north of Boot Heel area															
509	Tct	Big Burro	32.482	108.465	U	N	60.9	335.2	2.7						
689	Tdc	Steeple Rock	32.797	108.903	X	R	-55.5	167.1	3.9						
559	Tpu	Cliff	32.851	108.712	U	R	-52.8	166.0	2.6						
560	Tpu	Cliff	32.851	108.712	U	R	-54.3	155.0	1.8						
561	Tmt	Cliff	32.799	108.702	U	R	-18.2	168.6	11.7						
513	Tms5	Steeple Rock	32.783	108.937	U	R	-62.1	159.9	4.1						
690	Tmt9	Steeple Rock	32.758	108.879	U	R	-52.0	189.4	1.5						
511	Tk	Big Burro	32.476	108.447	U	R	-64.3	142.7	9.9						

Notes:
Fields left blank indicate analyses not done.
Facies: O = outflow, D = distal outflow (outside Boot Heel), C = intracaldera facies, L = lava, B = breccia, X = exotic facies (erupted outside Boot Heel field), M = minor or local units, U = unknown units
Paleomagnetic data: polarity: N = normal, R = reversed, T = transitional, inclination and declination are site mean direction, α95 is radius of cone of 95% confidence
$^{40}Ar/^{39}Ar$ data: mineral: san = sanidine, bio = biotite, plag = plagioclase analysis: F = resistance-furnace step heating, L = single-crystal laser-fusion, K/Ca is calculated from measured $^{39}Ar_K/^{37}Ar_{Ca}$
Unit name abbreviations explained in Tables 2 and 3, and as following for locations outside the borders of the Boot Heel field:
Little Hatchet Mountains: Tpp = tuff of Playas Peak (Zeller, 1970)
Steeple Rock area: Tam = tuff in andesite of Mt. Royal, Ttm5, Ttm8, Tmt9 = ash-flow tuffs, Tdc = Davis Canyon Tuff (Hedlund, 1990)
Cliff area: Tmt = quartz latite ash-flow tuff, Tmc = tuff of McCauley Canyon, Tct = tuff of Cherokee Canyon, Tpl, Tpu = lower and upper tuffs of Potholes Windmill (Hedlund, 1989)
Big Burro Mountains: Tct = ash-flow tuff, Tk = Kneeling Nun Tuff, Twtd = lithic ash-flow tuff (Hedlund, 1978)
Cedar Mountains: Tr + rhyolite ash-flow tuff (Thorman and Drewes, 1981)
Carrizalillo Hills: Ttl = lower rhyolite tuff, Tcl Tcu = lower and upper tuff of Carrizalillo Hills, Tj = tuff of Johnston Mountain (Seager and Clemons, 1988)